

# Plate Dynamics Near Divergent Boundaries: Geophysical Implications of Postrifting Crustal Deformation in NE Iceland

KOSUKE HEKI<sup>1</sup> AND G. R. FOULGER<sup>2</sup>

*Department of Geological Sciences, University of Durham, Durham, England*

B. R. JULIAN

*U. S. Geological Survey, Menlo Park, California*

C.-H. JAHN

*Institut für Erdmessung, Universität Hannover, Hannover, Germany*

The bulk of a tectonic plate is thought to move continuously at a rate consistent with the geologic average. On the other hand, movements are highly episodic at plate boundaries. We study the plate dynamics that relate to these two different modes by modelling the displacements observed using the global positioning system in Northeast Iceland 1987–1990. These observations were made about 10 years after an episodic divergent movement between the North American and Eurasian plates 1975–1981. The horizontal displacement field fits well a two-dimensional model of postrupture stress relaxation assuming a thin elastic layer overlying a layer of Newtonian viscosity. This analysis indicates values of about  $10 \text{ m}^2/\text{s}$  for the stress diffusivity and  $0.3\text{--}2 \times 10^{18} \text{ Pa s}$  for the Newtonian viscosity of the lower layer. However, no significant correlation exists between the observed and modeled vertical displacements probably because of the relative inaccuracy of the vertical component observations. Assuming that contemporary plate motion is the sum of many displacements that have diffused from boundaries where episodic displacements occur periodically, we simulate the spatial transition from episodic to continuous plate movements. The plate “boundary zone” where movements are episodic or quasi-episodic is of the order of 100 km wide, depending on the stress diffusivity (which may be fairly uniform throughout the world) and the frequency of episodic movements.

## INTRODUCTION

Since the beginning of the plate tectonic theory in the 1960s, it has been questioned whether plate movements are continuous or episodic. In the last decade, newly developed space geodetic techniques, especially very long baseline interferometry (VLBI), provided evidence that contemporary plate movements are continuous and have rates fairly consistent with those deduced for geologic time scales, e.g., the RM-2 [Minster and Jordan, 1978] and NUVEL-1 models [DeMets *et al.*, 1990]. The most frequent VLBI measurements have been made for trans-Atlantic baselines over the last 10 years [Carter and Robertson, 1989]. The variation of baseline lengths between European and North American radio telescopes is very smooth with no evidence for irregular plate movements. Pacific plate motion with respect to the surrounding plates has also been monitored at frequencies of up to once per month, and again, the velocities of these VLBI stations since 1984 are found to be constant [Heki *et al.*, 1990].

VLBI stations are generally located in the plate interiors with a few exceptions in the Western United States and Japan. The evidence for continuous plate motion is therefore strongest for plate interiors (Figure 1). In contrast, mo-

tions are known to be highly episodic at plate boundaries. Episodic motion accompanies earthquakes at convergent and transform fault boundaries and volcano-tectonic episodes at accretionary boundaries. Quantitative measurements are often available for such motions because of the long history of terrestrial geodetic surveying, e.g., trilateration and triangulation, around some subaerial plate boundaries.

A volcano-tectonic episode began in 1975 at the accretionary plate boundary in NE Iceland, and over the following decade was characterized by episodic divergent motion at the boundary between the North American and Eurasian plates [Björnsson *et al.*, 1977]. The NUVEL-1 model [DeMets *et al.*, 1990] predicts a  $0.94 \text{ cm/yr}$  half spreading rate in the direction N75W/N105E in NE Iceland. The plate boundary runs from Axarfjörður on the northern coast to the Vatnajökull ice cap and is known from the position of the neovolcanic zone (Figure 2). This contains several en echelon fissure swarms, each emanating from a central volcano, e.g., Krafla, Askja. The fissure swarms are thought to become active every 100 to 150 years [Björnsson *et al.*, 1979] when they experience episodic spreading motion of a few meters. One episode lasts for a few years and is followed by a quiescent period lasting until the onset of the next episode. The latest of these episodes, which commenced in December 1975, is known as the “Krafla rifting episode.” During the following decade a magma chamber beneath the Krafla volcano continuously inflated with occasional rapid deflations, when magma flowed out of the chamber and along the fissure swarm to form dikes. From 1975 to 1985 about 20 deflations occurred with diking and/or eruptions along the fissure swarm. From a few tens of centimeters to a few

<sup>1</sup>On leave from Kashima Space Research Center, Communications Research Laboratory, Hirai, Kashima, Ibaraki, Japan.

<sup>2</sup>Now at U. S. Geological Survey, Menlo Park, California.

Copyright 1993 by the American Geophysical Union.

Paper number 93JB00781.

0148-0227/93/93JB-00781\$05.00

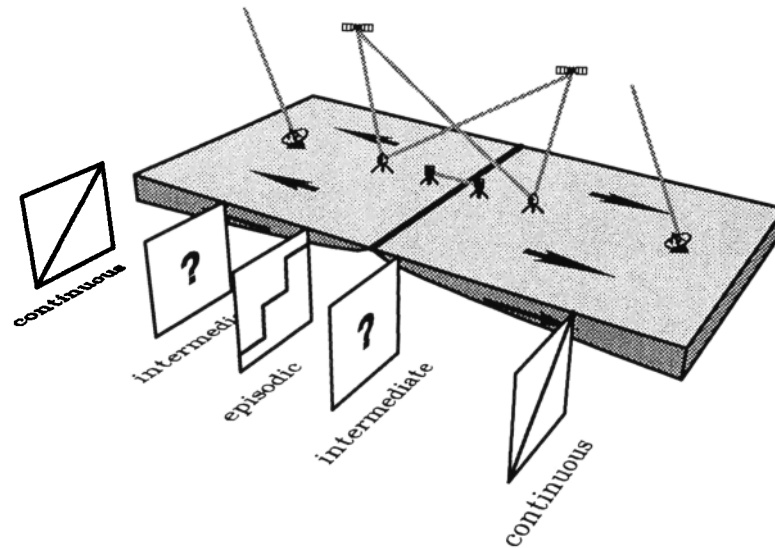


Fig. 1. Plate motion near an accretionary plate boundary. Although most of a plate moves continuously, movement is episodic at the boundary. Continuous movements have been measured using space geodetic tools, e.g., very long baseline interferometry (VLBI). Episodic movements have been monitored by conventional geodesy, e.g., triangulation, trilateration. Global positioning system (GPS) is a convenient tool to study the intermediate zone.

meters of local crustal widening accompanied each event, resulting in a total widening of up to 8 m in the center of the fissure swarm [Tryggvason, 1984; Wendt *et al.*, 1985].

In NE Iceland other similar volcano-tectonic episodes have occurred throughout history. The second most recent episode took place in the Askja volcano and its fissure swarm 1874–1875 [Sigurdsson and Sparks, 1978]. The third last episode, known as the “Mývatn fires,” occurred in the Krafla fissure swarm 1724–1729. At this time, the rifting was mainly concentrated south of the Krafla volcano, in contrast to the 1975 episode, which occurred mostly within and to the north of that volcano. Activity in the Theistareykir fissure swarm northwest of Krafla in 1618 is thought to have been a similar rifting episode [Tryggvason, 1984]. Although geodetic data documenting widening are not available for these old events, the recurrence intervals and the amount of opening during the 1975–1985 Krafla episode are quantitatively consistent with plate motion models.

Between plate boundary regions (e.g., NE Iceland) where motions are episodic and the plate interiors (e.g., Europe and eastern United States) where motions are continuous, a transition zone where movement is of intermediate nature would be expected (Figure 1). By studying how the episodic boundary movements grade into continuous movements across this transition zone, we may elucidate the physical processes controlling current plate motions and the physical properties of the lithosphere and asthenosphere in and around the boundary. An effective approach to this problem is to study the crustal behavior around the boundary during and after an episodic plate motion. In 1987 and 1990, about 10 years after the Krafla rifting episode, major geodetic surveys using the global positioning system (GPS) were carried out in NE Iceland. Early studies [Jahn *et al.*, 1992; Foulger *et al.*, 1992] report separation of the eastern and western flanks of the rift during 1987–1990 three times as large as that expected from rigid plate movements. Foulger *et al.* [1992] interpreted these movements as post-rifting relaxation of compressional stress accumulated in the flanking plates during the earlier rifting episode. We report here further

analysis of the GPS results and the simple stress relaxation model of Foulger *et al.* [1992] to clarify the structure and plate dynamics close to divergent plate boundaries.

In comparison, in the Asal-Ghoubbet rift, Djibouti, Africa, spreading of 60 mm/yr was detected during the period 1979–1986 using conventional ground surveying [Ruegg and Kasser, 1987]. Only 18 mm/yr is expected from the motion between African and Arabian plates. It is known that a similar “rifting episode” took place in 1978 there. Various kinds of geophysical and geological observations suggest similarity between that event and the recent Icelandic episode. The present study covers a much more extensive area because GPS was used and a much more complete picture of the deformation field was obtained.

Marine geophysical studies also reveal some morphological similarities between mid-ocean ridges and the neovolcanic zone in NE Iceland. On the Reykjanes Ridge southwest of Iceland, the submarine topography is characterized by a series of echelon ridge segments of similar dimensions to the subaerial central volcano/fissure swarm systems in NE Iceland [Johnson and Jakobsson, 1985]. The work we report from NE Iceland is therefore not only important as a unique tectonic study in Iceland but is also relevant to understanding worldwide accretionary plate boundaries.

## GPS IN NE ICELAND

### The Surveys

Large-scale GPS surveys were conducted in 1987 [Jahn *et al.*, 1990] and 1990 [Jahn *et al.*, 1992] to study crustal deformation in NE Iceland about 10 years after the Krafla rifting episode. Points were distributed throughout the eastern and western flanks of the Krafla fissure swarm (Figure 2). The network was dense within the fissure swarm and sparser points extended 130 km into the adjoining plates. Approximately 15 points were measured in and around the Askja fissure swarm and central volcano also (Figure 2). The northern part of the network lies within the Tjörnes Fracture Zone.

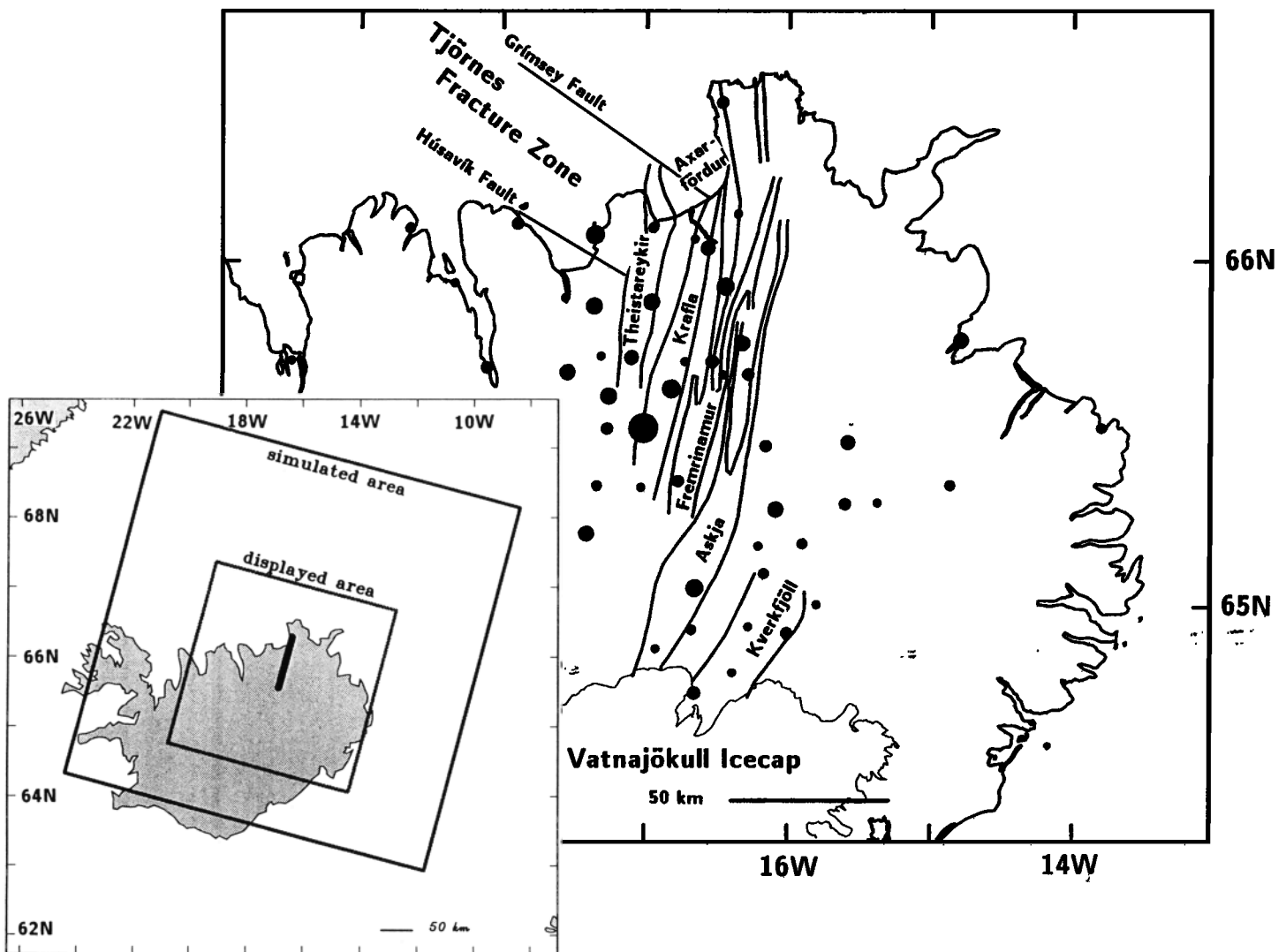


Fig. 2. The accretionary plate boundary between the North American and Eurasian plates crosses NE Iceland. The full spreading rate from the NUVEL-1 model [DeMets *et al.*, 1990] is 1.88 cm/year. The boundary is composed of several en echelon volcanic systems (containing central volcanoes and fissure swarms) such as the Krafla and Askja systems. Major GPS surveys of the points shown as circles were conducted in 1987 and 1990. Only GPS points measured successfully in both epochs are shown. The sizes of the circles are proportional to the square root of the number of measurements (the minimum number is two; one in 1987, the other in 1990). The network size is  $\sim 300$  km in the east-west and  $\sim 200$  km in the north-south. The northern ends of the fissure swarms connect with the Tjörnes fracture zone. Rectangular areas in the smaller map indicate the area used for the simulation studies ("simulated area") and that displayed in Figure 6 ("displayed area").

Seven TI-4100 GPS receivers were used for each survey. In 1987, a six-satellite morning observation window 3 hours 20 min long was used. In 1990, seven satellites were tracked during observation windows lasting 4 hours 10 min from midnight. In 1990 a small number of short additional observation sessions were used in the afternoon. Most of the points were measured more than once during each survey. Selective availability (SA), a deliberate degradation of the signal and broadcast orbit quality for civilian users, was in effect for the first two thirds of the 1990 survey. Carrier phases and P code pseudoranges were recorded for both the L1 (1.5 GHz) and L2 (1.2 GHz) frequencies to enable precise corrections to be made for ionospheric delays. Fifty-three sites were successfully measured in both 1987 and 1990 (Figure 2).

#### Data Analysis Procedure

The data were independently analyzed at the Universities of Durham (England) and Hannover (Germany) using different software packages to study the reliability of the results. *Jahn et al.* [1990, 1992] describe results obtained using GEONAP (Geodetic Navstar positioning) software [Wübbena, 1989]. The present paper describes the results obtained using the Bernese GPS software version 3.2 [Rothacher *et al.*, 1990] and compares the results from the two software packages.

For this work, the phase preprocessing (cycle slip detection and correction) part of the Bernese software, "MAUPRP," was replaced by "Turbo-Edit" [Blewitt, 1990]. Phase preprocessing constitutes two operations; (1) detecting cycle slips (identifying the epochs where cycle slips occurred) and

TABLE 1. Repeatability of Site Coordinates in the Three Components

Campaign	North-South	East-West	Up-Down
1987 (Ambiguity Fixed)	0.6	0.9	1.6
1987 (Ambiguity Free)	2.0	1.1	2.2
1990 (Ambiguity Free)	1.0	1.1	1.9

Units are centimeters.

outliers, (2) connecting cycle slips (determining the integer jumps in L1 and L2). Turbo-Edit uses so-called "wide-lane" linear combinations of the phases and pseudo-ranges in the first operation, and ionospheric linear combinations of the phases in the second operation [Blewitt, 1990]. Under quiet ionospheric conditions, both operations may be unproblematic and the two need not be separated. Under adverse ionospheric conditions, however, the second operation may become difficult. This is because ionospheric fluctuations may result in variations in the ionospheric delay of the order of the wavelengths of the L1 and L2 carriers on the time scale of the interval between measurements. Ionospheric fluctuations may be mistaken for cycle slips in such cases. The first operation, however, remains relatively easy because it is possible to cancel the ionospheric contribution by comparing the linear combinations of the phases and pseudo-ranges. In this study, identified cycle slips were corrected only when the phase ionospheric linear combinations were smooth enough to render reliable slip size estimations. Where the slip size could not be confidently estimated, the phase measurement was flagged. New initial phase ambiguities were then established at each such measurement when we proceeded to the next step, the formation of site-to-site single differences.

There was little difficulty in resolving the L1 and L2 ambiguities for the 1987 data. In the case of the 1990 data, however, although the differences between L1 and L2 ambiguities (the wide-lane ambiguities) were easily resolved, L1 and L2 ambiguity resolution was difficult. Possible reasons for this are (1) the shorter satellite arcs associated with each ambiguity to be resolved at the final parameter estimation stage, (2) poor broadcast orbits caused by SA, (3) ionospheric scintillations. The third factor is probably predominant. This is because the Bernese software relies on ionospheric (geometry-free) linear combinations of the carrier phase measurements and ionospheric corrections made using simple, single-layer, smoothly varying models to determine the L1 and L2 ambiguities. The efficiency of this method breaks down when the ionosphere is turbulent at the carrier wavelength level on the measurement interval time scale. In the case of the 1990 data, L1 and L2 ambiguity resolution was abandoned because of the danger of fixing ambiguities to incorrect integers, which would have resulted in degradation of the results over an ambiguity-free solution. As shown in the next section, the final ambiguity-free results of the 1990 survey are only slightly inferior to the ambiguity-fixed results of the 1987 survey.

A priori tropospheric delays for individual points were calculated and applied, assuming standard meteorological conditions at a reference altitude. Tropospheric parameters were not estimated because (1) the surface temperatures during both surveys were low ( $0^{\circ}$ – $10^{\circ}$ C) and unpredictable tropospheric delays caused by water vapor are thought to be small, (2) point separations in each session are relatively small (less than 100 km for most cases) and

tropospheric delays are almost cancelled when double differences are formed. In order to avoid multipath effects, we used relatively high elevation cutoff angles ( $15$ – $20^{\circ}$ ) and did not record low elevation signals which are required to discriminate between atmospheric delays and vertical point coordinates [Heki, 1990]. The introduction of atmospheric parameters into GPS data without sufficient low elevation observations increases the position uncertainty (mainly the vertical component) because of interparameter correlations. It is therefore often better not to estimate troposphere parameters unless their effect is very large (e.g., in the case of a hot, humid and nonuniform troposphere) [Heki et al., 1992]. Broadcast orbital information was used throughout the analyses. Baseline vectors and their covariances for each session were combined by a network adjustment technique [Heki, 1992] to produce a final set of site coordinates and a corresponding covariance matrix.

#### *Between-Session Site Coordinate Repeatability*

Both campaigns were conducted using seven receivers. In each session a reference point was occupied and one or two other points were common to the next or the previous session. We evaluate the between-session repeatabilities of the site coordinates using the weighted root-mean-square of the differences between the coordinates from the individual sessions and the network solution. These repeatabilities are compared for three solutions for the two surveys (Table 1). The 1987 results show a significant improvement in repeatability by ambiguity resolution. The repeatability of the 1990 ambiguity-free solution is slightly better than the 1987 ambiguity-free solution, possibly because of the longer observation windows and the more uniform sky coverage of the satellites in 1990. The dither process of SA in 1990 significantly degraded the code-derived absolute positions [Jahn et al., 1992]. However, the results shown in Table 1 suggest that SA scarcely affected phase relative positioning as far as coordinate repeatability is concerned.

#### *Between-Software Site Coordinate Repeatability*

The data were independently analyzed by University of Hannover using GEONAP software [Jahn et al., 1992]. Relative positions for the points using the same absolute coordinates of the reference point were compared for solutions from the two software packages. Both are ambiguity-fixed solutions for the 1987 survey. For 1990 survey two thirds of the ambiguities were fixed in GEONAP results. Neither analysis estimated tropospheric or orbital parameters. The weighted mean of the coordinate differences is 0.4, 0.9 and 2.9 cm in north-south, east-west and up-down components, respectively, for the 1987 survey and is 1.3, 3.1 and 4.0 cm in the 1990 survey. Figure 3 shows the Bernese positions relative to the GEONAP positions for all the points in 1987 and 1990.

For the 1987 data, the horizontal components are in very good agreement (within 1 cm for most sites) but the vertical

components are often different by a few centimeters (Figure 3a). This is caused mainly by the use of different atmospheric models. An incomplete atmospheric model is known to affect mainly the vertical position but the horizontal positions hardly at all [Heki, 1990].

For the 1990 data, differences of a few centimeters not only in the up-down but also in the east-west components are seen (Figure 3b). These average differences are all larger than the between-session coordinate repeatabilities in the Bernese solutions. The present results suggest that under adverse ionospheric conditions small differences in analysis procedures may result in greater differences in the coordinate results.

#### Comparison of the Results of the Two Surveys

We compared the final Bernese coordinate sets between the two surveys using a Helmert transformation, a transformation composed of translations/rotations along/about three axes (and scale transformation if necessary). In the network adjustment [Heki, 1992], because the three components of the baseline vectors were combined, we fixed only

the three components of a reference point and did not introduce reference directions. As a result of the transformation, significant translation was found ( $6\pm 6$ ,  $40\pm 6$  and  $11\pm 6$  mm in the  $X$ ,  $Y$  and  $Z$  axes respectively) which corresponds to the movement of the fixed reference point with respect to the center of gravity of the network. We remove such arbitrary biases in the displacement vectors when comparing them with those calculated using a geophysical model. Estimated rotations about the  $X$ ,  $Y$  and  $Z$  axes were  $0.05\pm 0.03$ ,  $0.11\pm 0.02$  and  $0.00\pm 0.02$  arcsec, respectively. Only the rotation about the  $Y$  axis (which is close to the local east-west axis in Iceland) is significant. This results from the subsidence of southern points (in the Askja region) with respect to the northern points. Because our network adjustment method does not require the removal of an arbitrary rotation, we consider that only translational biases are overprinted to the raw displacement vectors.

In the horizontal deformation field (Figure 4a), an arbitrary bias was added to enable us to clearly compare it with geophysical models given in the later sections. The results show a large systematic expansion perpendicular to the rift

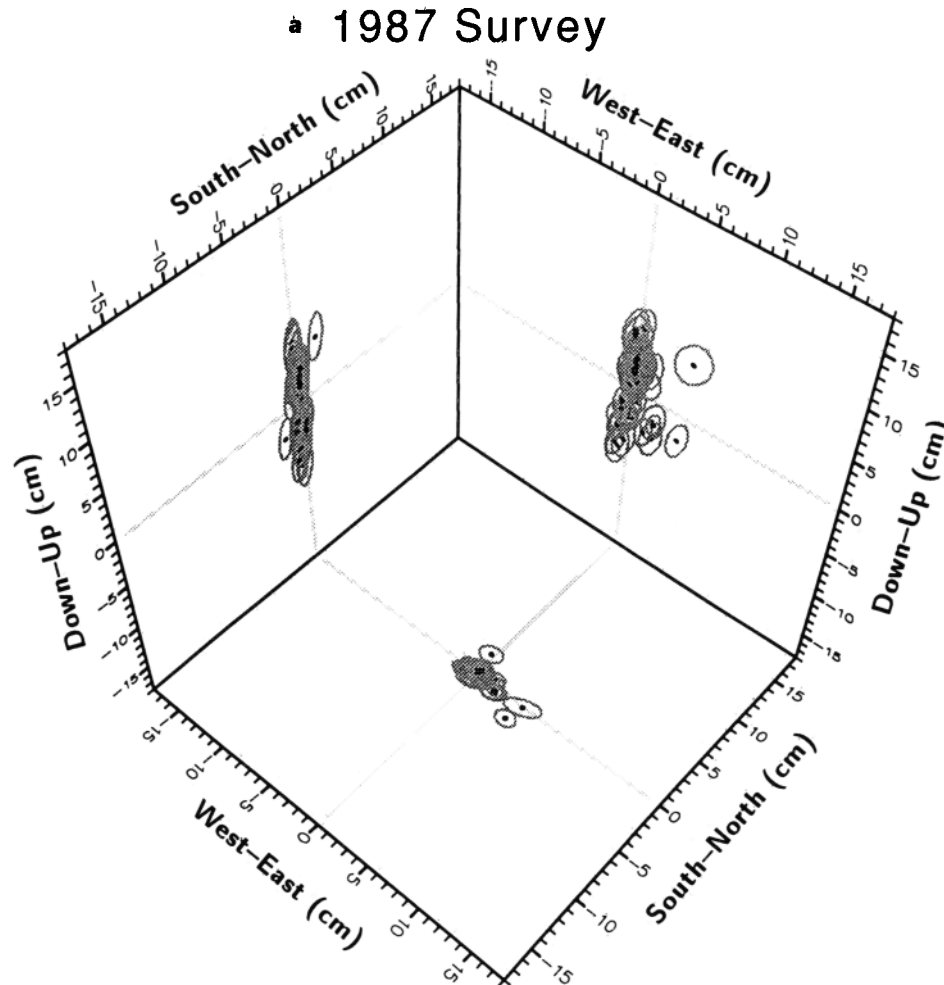


Fig. 3. Comparison of the final coordinates of the (a) 1987 and (b) 1990 survey between two software packages (the Bernese software [Rothacher et al., 1990] and GEONAP [Wübbena, 1989]). The Bernese positions are shown with respect to the GEONAP position [Jahn et al., 1992] at the origin. The  $1\sigma$  error ellipsoids shown refer to the Bernese results. They are projected onto a horizontal and two vertical planes. In the 1987 survey, the two solutions are very consistent in the horizontal components (average difference 4 mm in the north-south and 9 mm in the east-west). However, there are larger differences (average 2.9 cm) in the vertical component. In the 1990 survey, coincidence is good in the north-south (1.3 cm) but not very good in the east-west (3.1 cm) and the up-down (4.0 cm).

## b 1990 Survey

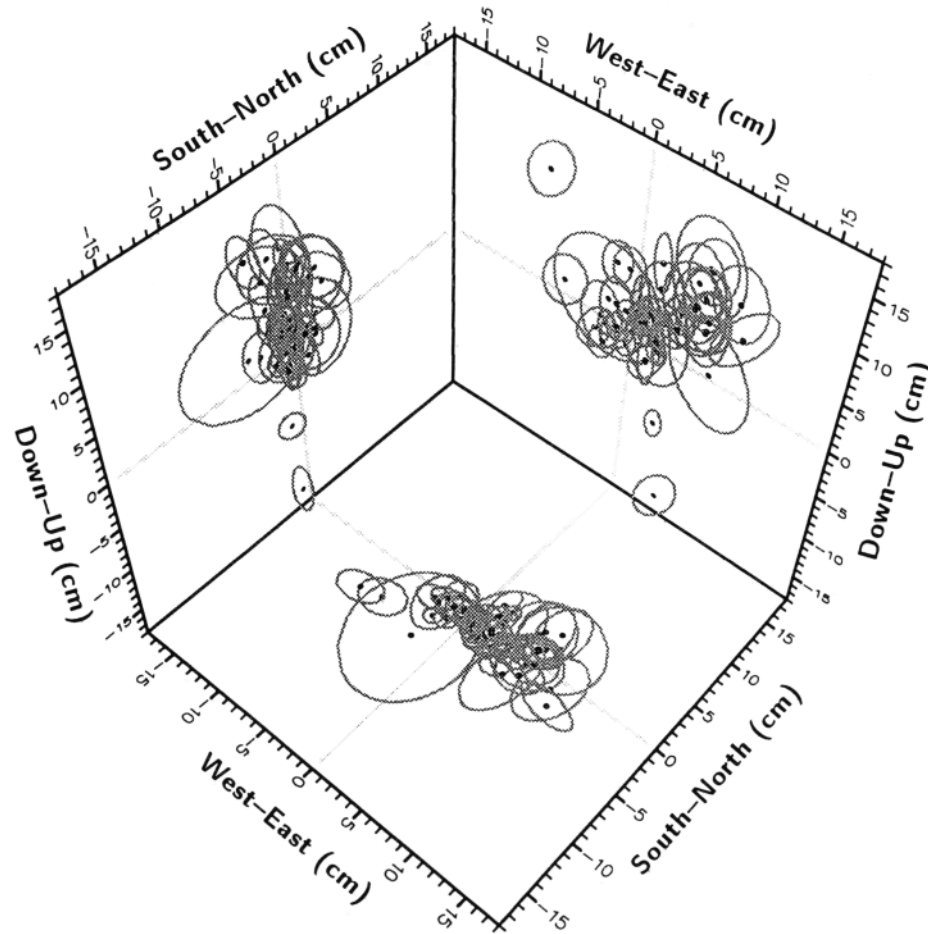


Fig. 3. (continued)

with an amplitude of approximately 15 cm, which is consistent with the earlier results of *Jahn et al.* [1992] and *Foulger et al.* [1992] obtained using GEONAP software. This is clearest around the middle of the fissure swarm, where the dike complex injected during the Krafla rifting episode was widest. East-west movements are at their maximum a few tens of kilometers from the central axis, and the movements of points further away are smaller. A smaller component of expansion parallel to the rift is also observed and results in a radial pattern of displacement. Displacements of the southerly points of the network (in the Askja region) are much smaller and have a southward trend with respect to the points in the Krafla region.

Vertical displacements (Figure 4b) are of the order of a few centimeters. The southerly points (in the Askja region) subside with respect to the more northerly points (in the Krafla region). Within the Krafla region, the vertical movements are less systematic than the horizontal but there is some tendency for the points near the rift axis to either uplift or subside while those farther to the east and west of the axis are generally uplifted.

#### GEOPHYSICAL MODELS OF POSTRIFTING CRUSTAL DEFORMATION

Major tectonic activity commenced in the Krafla system in 1975, and intense diking subsequently occurred at inter-

vals of a few months. A change in the style of tectonism occurred in the middle of 1980, after which time activity was mainly eruptive [*Einarsson*, 1991]. Evidently, the minimum principal stress along the plate boundary had increased such that it could support a column of magma extending to the surface, thus precluding further diking. The last eruption occurred in September 1984 and only intermittent inflation was detected after 1985.

The time-averaged full spreading rate in NE Iceland is about 1.9 cm/year [*DeMets et al.*, 1990] and this can explain less than half of the observed deformation (Figure 4a). *Foulger et al.* [1992] interpreted the deformation as the response of the shallow elastic crust to the 1975–1981 spreading episode, delayed by mechanical coupling with an underlying viscous layer, i.e., the relaxation of compressional stress generated 1975–1981 in the flanking plates [*Elsasser*, 1969; *Bott and Dean*, 1973]. The present study develops this theory by expanding the original one-dimensional model of *Foulger et al.* [1992] to the two-dimensional case and modelling the whole observed displacement field.

#### Comparison Between the Simulated and Observed Deformation

The mathematical procedure to generate simulated displacement fields for the period 1987–1990 is given in detail in the appendix. We compare these simulated displacement

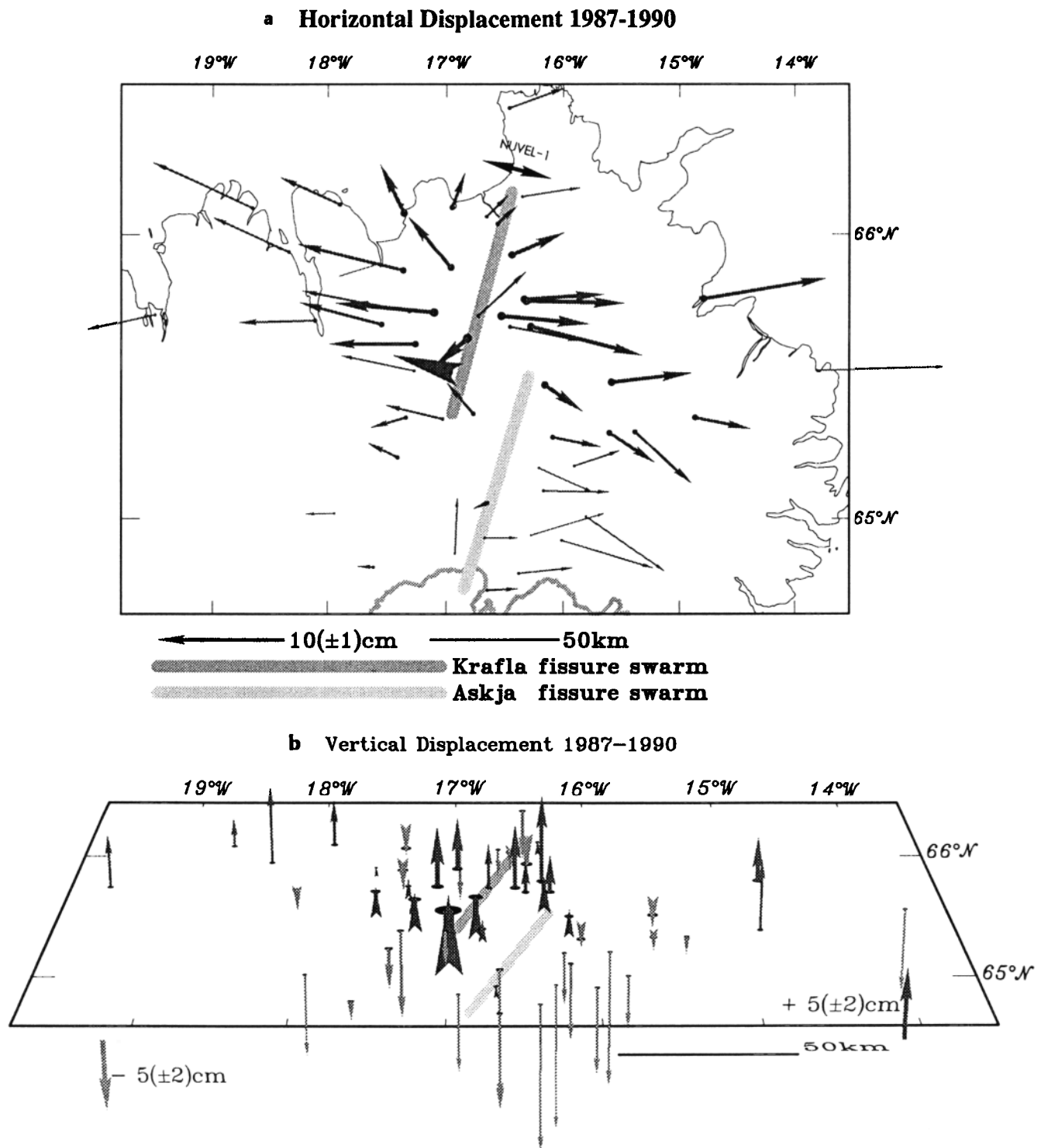


Fig. 4. Displacements of the GPS point between 1987 and 1990 (Bernese software). (a) The same translation as is applied in Figure 6 is applied here and (b) an average translation along the vertical axis is removed in vertical displacements. The thicknesses of the arrows are proportional to the inverse of the errors in the displacement vector lengths. The arrow in Figure 4a shown in the legend shows a displacement of 10 cm and an error of 1 cm. The two arrows in Figure 4b shown in the legend show upward and downward displacements of 5 cm and errors of 2 cm. The shaded lines denote the Krafla and Askja fissure swarms. In Figure 4b downward vectors are discriminated from upward vectors by the lighter tones of the arrows. The black arrow in the northern part of Figure 4a denotes the displacement vector expected in 3 years period by the NUVEL-1 plate motion model [DeMets et al., 1990].

vectors with those observed using GPS. The ratios of the three diffusion coefficients of equation (A10) are taken as known and their absolute values are determined by modelling the observed displacements. Movements at the precise

locations of the GPS points are obtained by interpolating within the finite difference grid. Because GPS phase positioning is relative, translational biases in the observed displacements are estimated by the least squares method when-

ever we compare two sets of vectors. The weighted root-mean-square (WRMS) is calculated to evaluate the overall goodness of fit, and its square is defined as

$$\text{WRMS}^2 = \frac{\sum_{i=1}^N (u_{obs,i} - u_{sim,i})^2 / \sigma_{u,i}^2}{\sum_{i=1}^N (1/\sigma_{u,i}^2)} + \frac{\sum_{i=1}^N (v_{obs,i} - v_{sim,i})^2 / \sigma_{v,i}^2}{\sum_{i=1}^N (1/\sigma_{v,i}^2)} \quad (1)$$

where  $N$  is the number of points compared and  $u, v_{obs}$  and  $u, v_{sim}$  are the observed and simulated  $u, v$ . Variables  $\sigma_u$  and  $\sigma_v$  are the formal standard errors of the observed displacements in the  $x$  and  $y$  directions. The goodness of fit for the  $x$  and  $y$  components is evaluated using the normalized root-mean-square (NRMS), where

$$\text{NRMS}_x = \sqrt{\frac{\chi^2}{\nu}} = \sqrt{\frac{\sum_{i=1}^N (u_{obs,i} - u_{sim,i})^2 / \sigma_{u,i}^2}{N-1}} \quad (2a)$$

$$\text{NRMS}_y = \sqrt{\frac{\chi^2}{\nu}} = \sqrt{\frac{\sum_{i=1}^N (v_{obs,i} - v_{sim,i})^2 / \sigma_{v,i}^2}{N-1}} \quad (2b)$$

The number of degrees of freedom,  $\nu$ , is equal to the number of observations  $-1$  because the network translation in the horizontal plane was estimated. These three statistics are plotted in Figure 5 for different values of  $\kappa_1$ . Points within 10 km of the dike are not included in the calculations (shown with open arrowheads in Figure 6) because we expect our thin-plate approximation to be increasingly inappropriate close to the rift axis. A distinct minimum exists for the WRMS at  $\kappa_1 \approx 10 \text{ m}^2/\text{s}$ . A similar minimum occurs for the  $\text{NRMS}_x$ .  $\text{NRMS}_y$  does not show a clear minimum but the fit is good ( $\text{NRMS}_y \approx 1$ ) for all the diffusivity values. We

therefore consider  $10 \text{ m}^2/\text{s}$  the best estimate for the stress diffusivity in NE Iceland. The same calculation was done taking  $\lambda = 0.5\mu$  and this gave almost the same results for the diffusivity and goodness of fit. However, this procedure gave an estimation of the viscosity of lower layer that was different by about 10 percent (see next section).

The NRMS should be close to unity, provided both the model and the formal errors of the observational data are appropriate. Values of about 1.8 ( $x$  axis) and 1.2 ( $y$  axis) were obtained in this study and this may be considered fairly good. However, their differences from unity suggest a certain amount of model defect and/or underestimated observational errors. Figure 6 compares the observed displacement vectors with those simulated using the "best" values for  $\kappa_1, \kappa_2, \kappa_3$  in equation (A10). The residual vectors (observed vectors minus simulated vectors) are shown in Figure 7a.

The most notable feature in Figure 7a is that the points near the Krafla central volcano display a symmetric radial pattern outgoing from the volcano ( $x = y = 0$ ). This probably is attributable to the effect of the inflation of the magma chamber beneath the central volcano. At the start of the episode, there was a 7 mm/day uplift at the center of the inflation [Björnsson, 1985], which decayed down to an average of about 0.3 mm/day during 1980–1989 (A. Björnsson, personal communication, 1992). Such an inflation of the magma reservoir would result in an areal expansion that would generate outward propagating radial displacements.

The solution to equations (A10) for the radial displacement  $u_r$  at a distance  $r$  and time  $t$ , caused by an areal expansion of  $A$ , occurring at  $r = 0$  and time  $t = 0$ , is given by

$$u_r(r, t) = \frac{A}{2\pi r} \exp\left(-\frac{r^2}{4\kappa t}\right), \quad (3)$$

with  $\kappa$  as defined in equation (A3). Figure 7b shows the

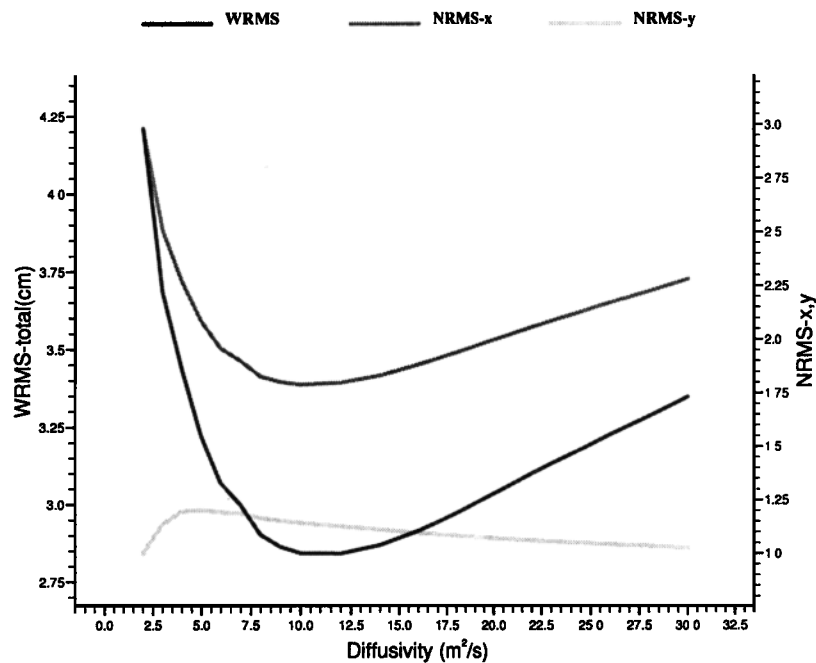


Fig. 5. Changes in statistics indicating goodness of fit between observed and simulated displacements 1987–1990 for various values of the diffusivity  $\kappa_1$ . There is a minimum around  $10 \text{ m}^2/\text{s}$ . Goodness of fit for two components together ( $x$  and  $y$ ) are consistent with the total WRMS. The points within 10 km from the dike are excluded in the calculation of these values.



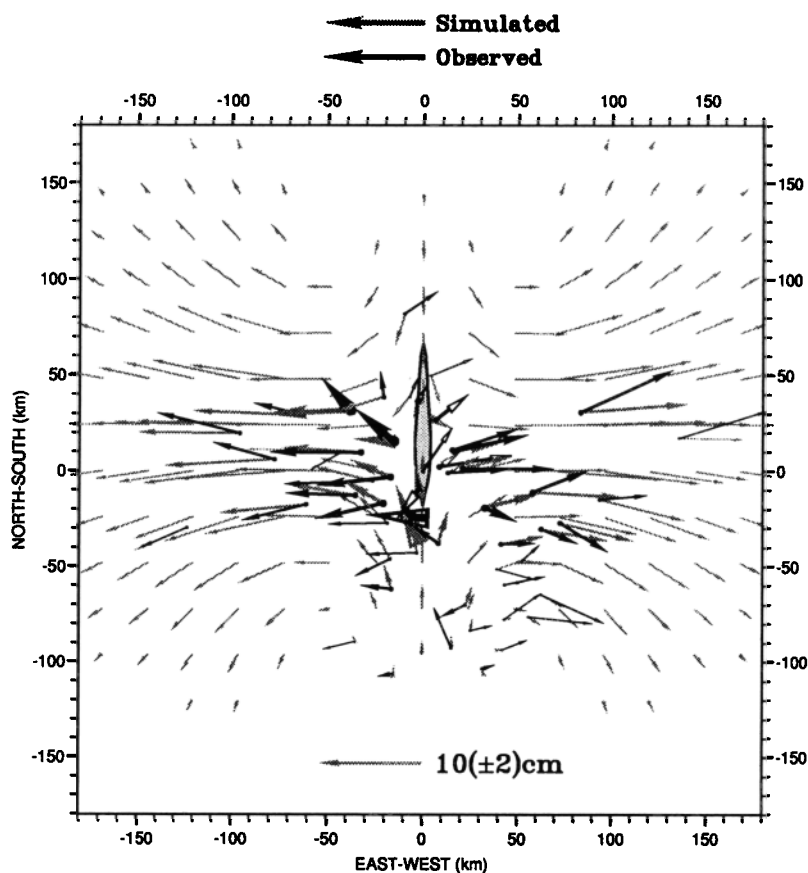


Fig. 6. Comparison between the observed and simulated displacements 1987–1990 for the “best” stress diffusivity,  $\kappa_1 = 10 \text{ m}^2/\text{s}$ , obtained from Figure 5. Shaded arrows represent simulated data and solid arrows observed. The simulated arrows are given at grid points with 24-km separation in addition to at the GPS points. Simulated arrows at grid points are shown only when they are more than 1 cm. Widths of the observed arrows are inversely proportional to the errors (thin arrows are less significant). The overall fit is fairly good but certain areas (e.g., near the central volcano and in the Tjörnes Fracture Zone) show large discrepancies. The points within 10 km of the dike which are excluded in fitting the data are shown with open arrowheads. Only a part of the area in Figure 2 (the “displayed area”) is shown in this figure.

displacement field 1987–1990 calculated using equation (3). A diffusivity  $\kappa$  of  $10 \text{ m}^2/\text{s}$  was used. The time of expansion and the amount of expansion  $A$  are determined to best explain the residual vectors in Figure 7a, which are the middle of 1987 and  $4000 \text{ m}^2$ , respectively. If we add these displacement vectors to the simulated vectors, the  $\text{NRMS}_x$  and  $\text{NRMS}_y$  are improved to about 1.6 and 1.0, respectively (these improvements are, however, not significant at the 95 percent confidence level according to the  $f$  test).

Although there was a continual supply of magma to the reservoir 1975–1985, much was also drained out to create dikes and to form lava flows. Such deflations caused areal contractions which largely cancelled out the preceding expansions and therefore the outgoing movements. The inflation responsible for the radial movements we observe 1987–1990 must be only that which occurred after the land inflated permanently past its pre-tectonic height, in the mid 1980s. Assuming constant inflation rate during the early 1980s (an approximation since the inflation has in fact been quite episodic since early 1985 (*P. Einarsson*, personal communication, 1992)) and a radius of the magma chamber of 2–3 km,  $4000 \text{ m}^2$  corresponds to the areal expansion in 3–4 years. Some minor inflation episodes occurred during the period 1987–1990 and elastic response to them may also be

to some extent responsible for the observed displacements.

Another area where the fit is relatively poor is the north-west. These points are located within the Tjörnes Fracture Zone [*Saemundsson*, 1974], which is a complex of minor rifts and strike-slip faults. Right-lateral transform motion is taken up there by a series of parallel NW-striking faults or seismic zones (for example, the Húsavík fault and the Grimsey fault) which are characterized by frequent earthquake swarms [*Einarsson*, 1991]. Motion on these structures has probably modified the deformation field after the spreading episode.

It is interesting to note that the northernmost point moved eastward although it appears to be west of the extension of the Krafla fissure swarm. This point is north of the fracture zone, i.e., it is on the Eurasian side of the plate boundary, so the observed displacement is reasonable from a plate tectonic point of view. In the southern part of the network (the Askja system), the boundary between eastward-moving and westward-moving points lies somewhat east of the Krafla fissure swarm, and corresponds to the Askja fissure swarm (Figure 4a). These complexities suggest that the stress relaxation we observe might be modeled better still by taking account of the several discrete tectonic units within our network.

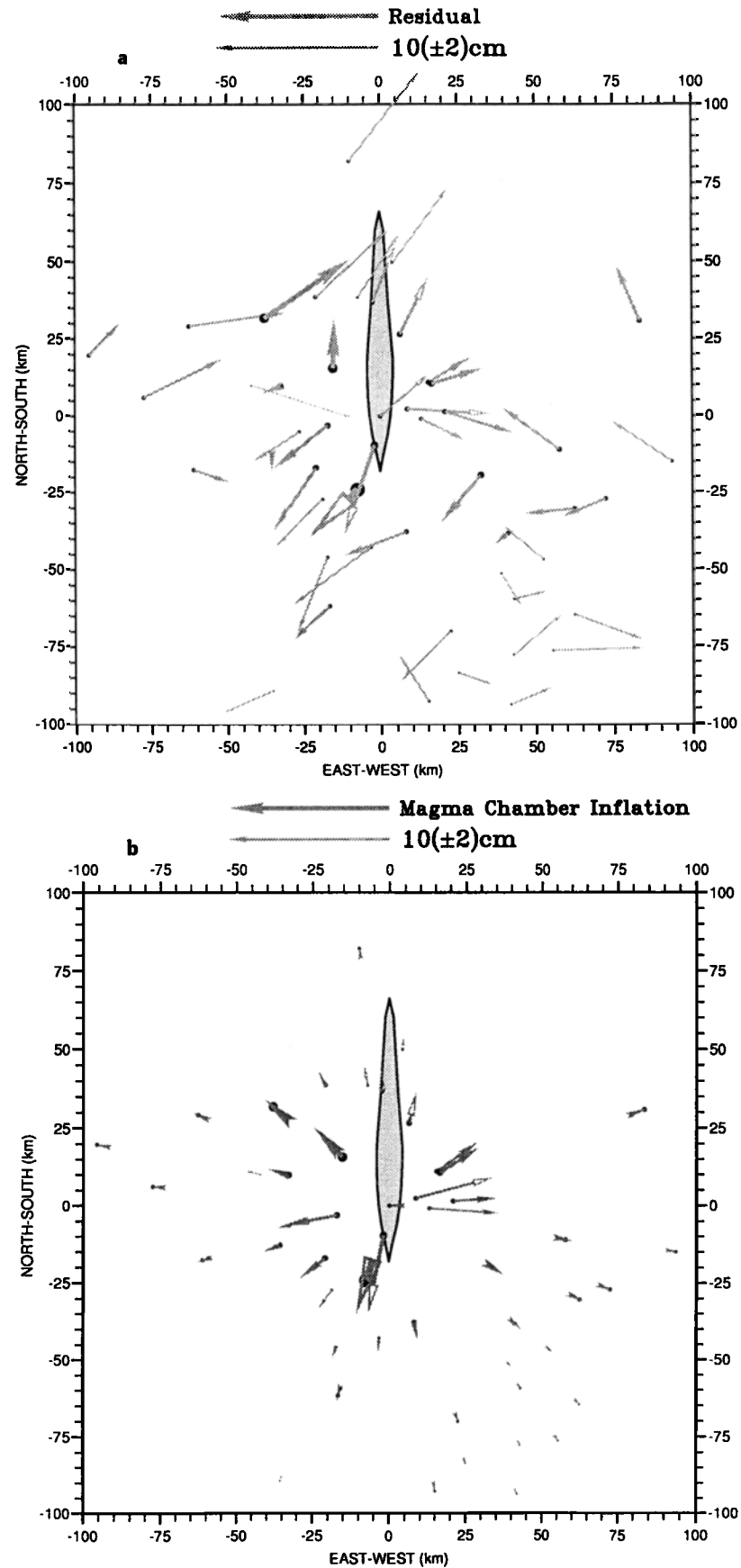


Fig. 7. (a) Residual vectors, i.e., the differences between the observed and simulated vectors in Figure 6. The implications of the open arrowheads and arrow broadness are the same as in Figure 6. There is a systematic radial outgoing pattern near the Krafiá central volcano, which is explained by recent magma chamber inflation. (b) Displacements 1987–1990 calculated using equation (3) and the same diffusivity as in Figure 6,  $4000 \text{ m}^2$  as an areal expansion and 1987 as the time of expansion.

In addition to these tectonic complexities the following factors may be responsible for the unmodeled discrepancies observed in Figure 6; (1) inaccuracy of the assumed dike widths including vertical nonuniformity, (2) anisotropy and nonuniformity of the stress diffusivity, (3) viscoelasticity or other more complex rheology, (4) remnants of past spreading events, e.g., the Askja rifting episode in the last century and the Mývatn Fires in the Krafla system in the 18th century.

Variation of the dike widths with depth is difficult to estimate, but the model adopted here is acceptable considering the goodness of the fit. The elastic upper crust is thought to be exceptionally thin in the neighborhood of the Krafla central volcano [Björnsson, 1985] and the stress diffusivity is therefore likely to be nonuniform in the study area. Incorporation of an accurate map of elastic layer thickness could probably be used to improve our fit. In the case of the third factor, we assumed thinness and perfect elasticity for the upper layer and Newtonian behavior for the lower layer. These approximations also affect the fit and the estimated stress diffusivity. A model incorporating viscoelasticity would result in improvement. Factor (4) is discussed later.

#### *Stress Diffusivity and the Viscosity of the Newtonian Layer*

Foulger *et al.* [1992] analyzed the 1987–1990 Krafla deformation data using a one-dimensional stress diffusion model and obtained a diffusivity estimate that is smaller than ours by nearly an order of magnitude. In their study the data in a narrow zone directly to the east or west of the central part of the dike were used. In this zone, most of the GPS points with good data quality (therefore with higher weights in estimating the diffusivity) are within a few tens of kilometers. However, the present analysis suggests that these points are most affected by the radial outward displacements due to the inflation of the Krafla magma reservoir. Ignoring this deformation source leads to an underestimate of the diffusivity because of the relatively large velocities still remaining in the vicinity of the fissure swarm. However, this factor does not entirely account for the discrepancy, and it is likely that there is a real spatial variation in diffusivity in NE Iceland, a conclusion that agrees with known structural variations in the region.

Magnetotelluric measurements reveal the presence of a relatively thin layer of high conductivity underlying NE Iceland [Beblo *et al.*, 1983; Björnsson, 1985]. The top of this layer lies at depths of 8 to 10 km beneath the axial rift zone, increasing to 20 km away from plate boundary. Foulger *et al.* [1992] suggest that this layer may be the same as the viscous layer of our model, and calculate a viscosity of  $0.3\text{--}2 \times 10^{19}$  Pa s using their estimate of  $1 \text{ m}^2/\text{s}$  for  $\kappa$ . Our two-dimensional analysis suggests a value of diffusivity 10 times larger than this initial estimate, and this suggests a revised estimate of the viscosity of the viscous layer of  $0.3\text{--}2 \times 10^{18}$  Pa s. This extremely low value is in better agreement with the findings of Sigmundsson [1991] who estimates an average value of  $10^{19}$  Pa s or less for the viscosity of the asthenosphere “as a whole” beneath Iceland from postglacial rebound.

Magnetotelluric measurements and the present study are consistent with a relatively thin elastic layer underlain by a layer of unusually low viscosity. These two factors compensate for each other so it might be expected that the diffusivity (which is proportional to  $h/\eta$ ) is similar to that in

other regions. Generally speaking, since thinner lithosphere might be expected to be underlain by less viscous (hotter) material it might be anticipated that the stress diffusivity varies less than either  $h$  or  $\eta$  do throughout the world.

#### *Sources of Error*

Our results hinge on several simplifying assumptions and approximations that can not be eliminated with current knowledge. The computed viscosity depends on the thicknesses of the elastic and viscous layers, which we infer from magneto-telluric results. These values are relatively poorly resolved. Furthermore, the thickness of the upper, low-conductivity layer (which we identify with the elastic layer) increases markedly with distance from the spreading plate boundary, and we have quoted the results for the two end-member values only.

Our model involves several physical simplifications. In particular, Newtonian behavior for the viscous layer would (unrealistically) prevent any elastic response at the time of dike intrusion and overestimate the motions at later times. Theoretical results calculated by Savage and Prescott [1978] (their Figures 1 and 2), however, indicate that for the distances and times appropriate to our data the assumption of Newtonian viscosity gives results similar to those for Maxwellian viscoelasticity. In any case, both viscous and viscoelastic laws are idealizations of the actual behavior of the Earth. Constitutive parameters derived from these laws must be interpreted in terms of the behavior of real materials for the appropriate time scales and strain rates [Ranalli, 1993].

One of the largest sources of uncertainty in our model relates to the kinematic assumptions about flow in the viscous layer. We assume that the velocity-depth relation within this layer is linear. Other assumptions, such as a quadratic relation giving no net transport through a vertical section [Bott and Dean, 1973], will affect the traction-velocity relation at the base of the elastic layer, and hence decrease the inferred viscosity by as much as an order of magnitude [Ranalli, 1993]. Such an assumption would be appropriate if transient motions of the elastic layer were accompanied by transient counterbalancing flow in the viscous layer. This in turn depends on such factors as the sources and transport mechanism of the material that forms newly created lithosphere, about which current knowledge is sparse.

#### *Vertical Crustal Movements*

Equation (A11) suggests that subsidence is proportional to the areal dilatation  $\Theta'$ , that is  $\partial u/\partial x + \partial v/\partial y$ . Figure 8 shows  $-\Delta\Theta'$  for the period 1987–1990 simulated using the best fit parameters (the effect of the magma chamber inflation is not included). It is expected that points near the rift subside while points in the outer regions rise by a smaller amount. Figure 4b shows slight uplifts for the easternmost and westernmost points (about 100 km apart from the rift), slight subsidences for the medium distance points (a few tens of kilometers from the rift) and a mixture of subsidence/uplift within a few tens of kilometers from the rift. These observations are crudely consistent with Figure 8 if we allow for complexities near the rift due to the effect of the magma chamber. However, the correlation between the observed and computed uplifts is statistically insignificant because of large uncertainties in the vertical positions in GPS geodesy.

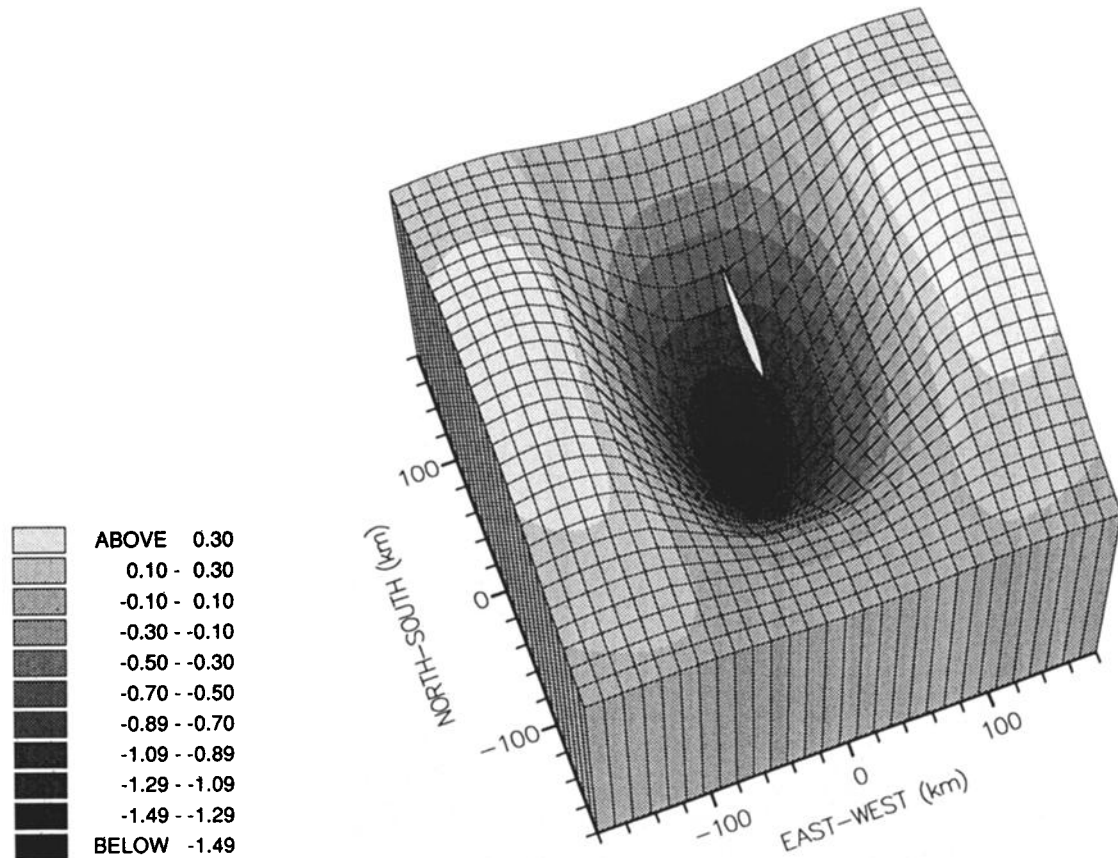


Fig. 8. Expected contraction in the horizontal plane ( $-\Theta' = -\partial u/\partial x - \partial v/\partial y$ ) 1987-1990 according to the simulation result with  $\kappa_1=10 \text{ m}^2/\text{s}$ . The unit displayed is  $10^{-6}$ . The area near the rift axis is expected to subside while the outer area about 100 km from the axis is expected to uplift by a smaller amount.

#### PLATE DYNAMICS NEAR THE DIVERGENT PLATE BOUNDARY

We discussed the propagation of episodic boundary motions into the plates in the previous section. We now return to our original question, what is happening in the “intermediate” zone of Figure 1? The solutions of the one-dimensional model (equations (A4) and (A5)) are pertinent to this question.

Near the boundary, a rifting event causes a sudden displacement, similar to a step function (Figure A1) and a “pulse” of velocity (Figure A2). The individual pulses become smoothed as they propagate into the plate, in whose deep interiors many past events have been “stacked,” resulting in apparently constant motion. By treating episodic boundary motions as a repeating phenomenon, we infer resultant crustal behavior.

Rifting episodes have been occurring in NE Iceland for the last 4 Ma [Saemundsson, 1974]. Taking the time interval of 100–150 years [Björnsson, 1985], 30 to 40 thousand episodes may have occurred in total. The current displacement (since rifting began)  $U(x, t)$  is the sum of the contribution of the latest episode  $u(x, t)$  and of a large (essentially infinite) number of past episodes (hereafter called the “background” movement)

$$\begin{aligned}
 U(x, t) &= u(x, t) + u_{\text{background}} \\
 &= u(x, t) + \sum_{n=1}^{\infty} u(x, t + nT)
 \end{aligned}
 \quad (4)$$

where  $T$  is the recurrence interval of the events.

$U(x, t)$  is infinitely large and is meaningful only when treated as a difference with respect to a certain reference epoch, i.e.,  $U(x, t) - U(x, t_0)$ . Figure 9a–d shows the displacement with respect to time  $t = 0$  as functions of time  $t$  for four different distances from the rift axis ( $x = 25, 50, 100$  and  $200$  km). We assumed 1 m for the half dike width  $U_0$  and 100 years for the repeat interval  $T$  so that the time-averaged half spreading rate is 1 cm/year.  $10 \text{ m}^2/\text{s}$  is used for stress diffusivity  $\kappa$ .

The velocity fluctuates with time. It increases immediately after an episode and subsequently decreases. This tendency is most marked in Figure 9a (closest to the boundary) where the motion is almost purely episodic, that is, substantial movements occur only for a short period after an episode and there is little movement just before the onset of a new episode. In Figure 9b (50 km from the boundary), because stress relaxation takes more time, episodicity is less pronounced, that is, there is recognizable continuing movement just before a new episode. In Figure 9c (100 km from the boundary), movement becomes more continuous with only small “ripples” apparent. Plate motion is nearly constant 200 km from the boundary (Figure 9d). This pattern of motion may be similar to the “plate motion” observed using VLBI between European and North American stations.

The plate functions as a reservoir for horizontal stress and strain and its own movement is constant regardless of how episodic movements occur along the boundary. Episodic movements at opposite ends of the plate (i.e., the spread-

ing boundary and the subduction zone) are thereby isolated from each other and, as suggested by *Bott and Dean* [1973], no temporal or spatial relationship exists between them. Figure 9 also predicts that a space geodetic measurement of the plate velocity (perhaps spanning a window of a few years) may be corrupted from "true" time averages, e.g., NUVEL-1 [*DeMets et al.*, 1990] when stations near plate boundaries are used.

The "background" crustal velocity  $\partial u_{background}/\partial t$  gives a further insight into the dynamics of a plate boundary. The "background" velocity shown in Figure 10 is the crustal movement just before the onset of a new spreading episode. The velocity is zero at the axis and approaches the averaged half spreading rate (1 cm/year) with distance. Imme-

diately prior to a spreading episode it would be expected that the baseline lengths would increase steadily at a time-averaged rate when measured between points in the plate interiors. No appreciable expansion would be measured over short lines even if they span the plate boundary. *Möller and Ritter* [1980] report horizontal contraction across the Krafla system of approximately 0.5 m 1965–1971 using conventional ground geodetic survey techniques. This is inconsistent with the present study and might be caused by undetected observation errors, as the authors of that paper themselves suggest [*Wendt et al.*, 1985].

The characteristic "width" of the intermediate zone (Figure 1), defined as the zone where the background velocity is less than one half of the time average, is about 130 km for

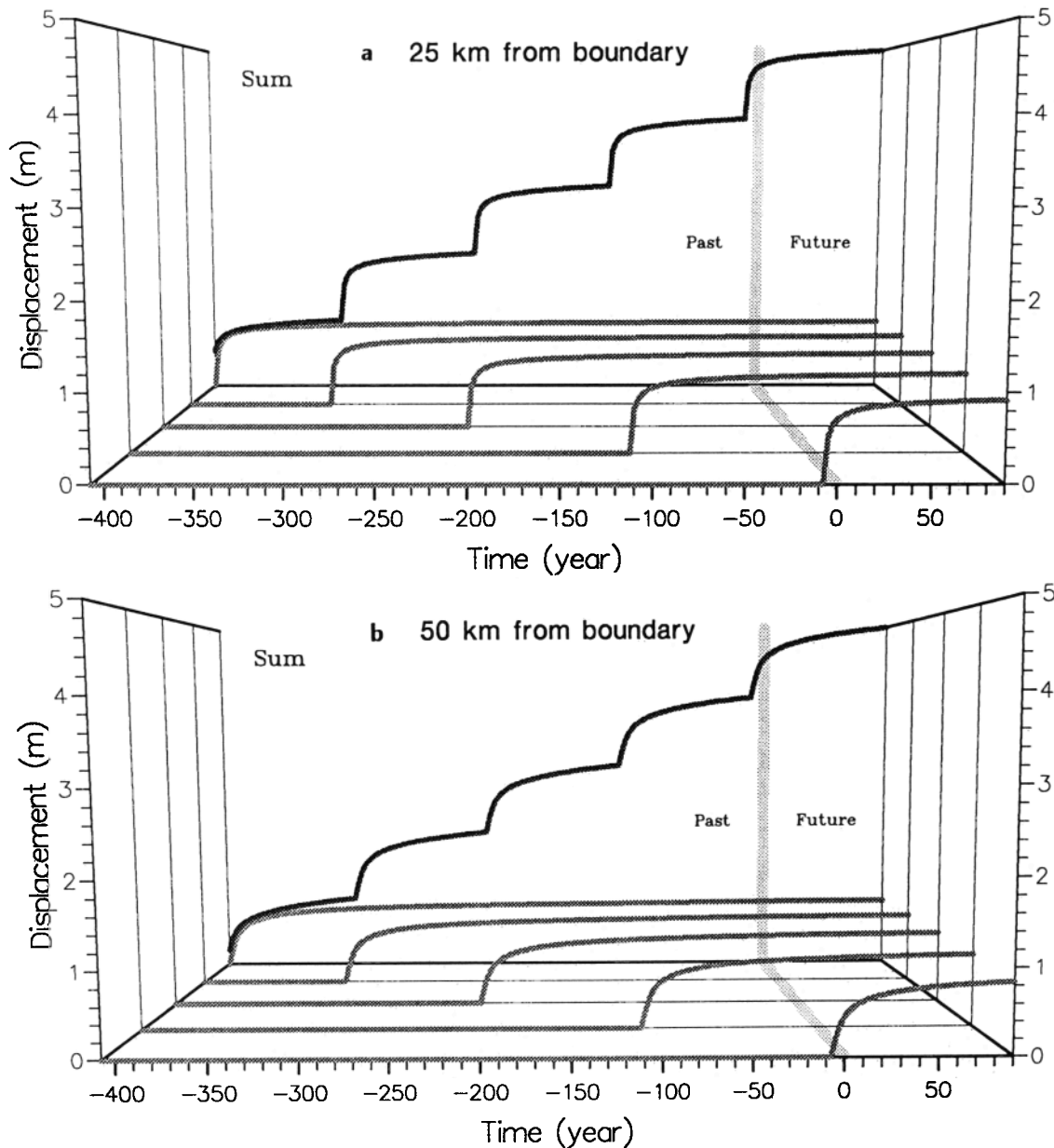


Fig. 9. Displacement versus time at points (a) 25 km, (b) 50 km, (c) 100 km, and (d) 200 km from the plate boundary. It is assumed that a rifting event occurs every century. The last one is assumed to have occurred 10 years ago so that at present ( $t = 0$ ) we are observing an early phase of the stress relaxation of the last episode. Dike half width is assumed to be 1 m so that the average half spreading rate is 1 cm/year. Displacements caused by each of five recent episodes are shown by light gray lines. The dark gray line is the sum of these five episodes and innumerable past episodes. Its value is reset to zero at the onset of the fifth last episode. Stress diffusivity  $\kappa$  is set to  $10 \text{ m}^2/\text{s}$ . Movements change from episodic to continuous with distance from the plate boundary.

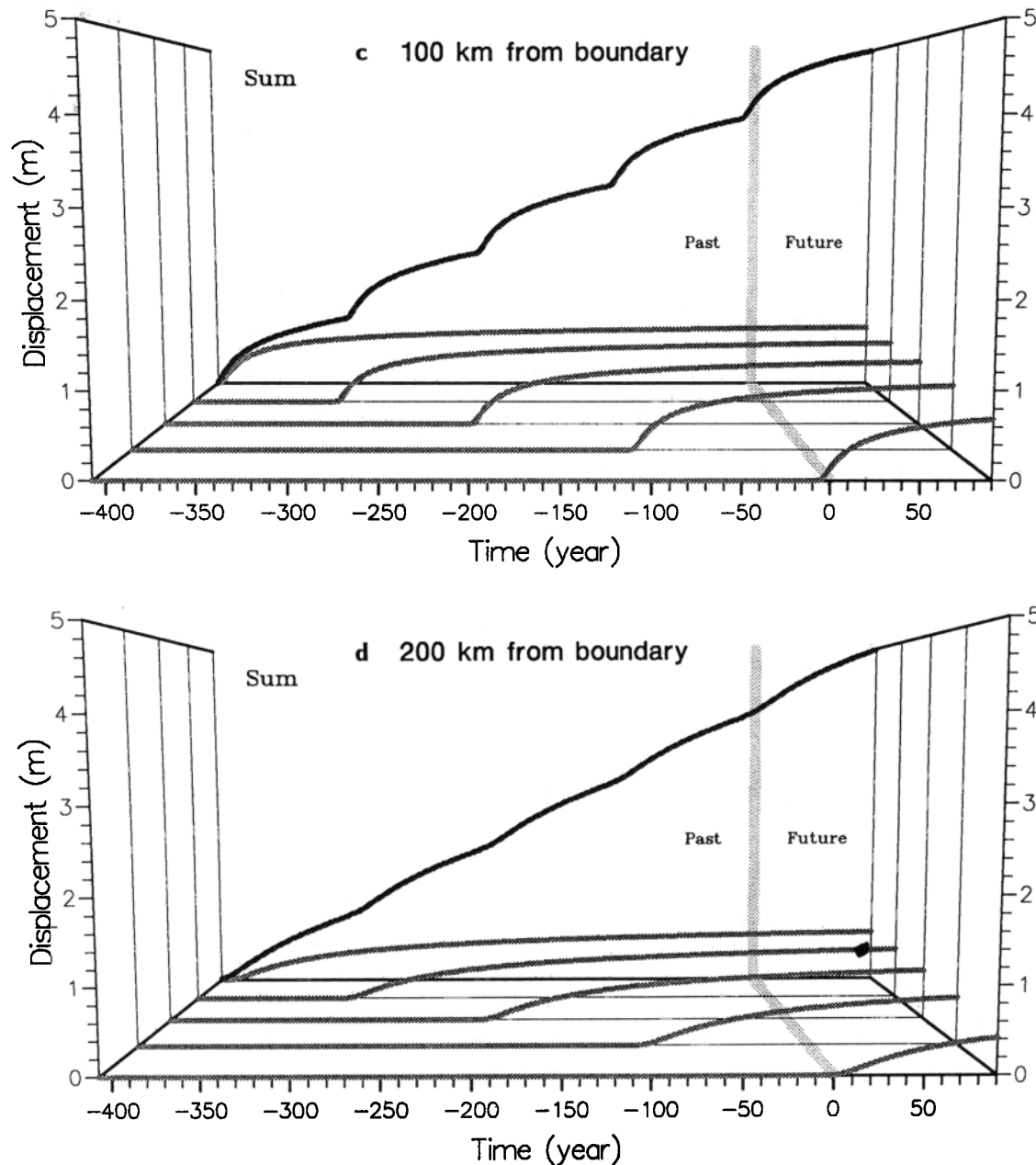


Fig. 9. (continued)

NE Iceland. This width is controlled by the recurrence interval  $T$  (and hence amount of episodic movement  $U_0$  required to maintain the averaged plate velocity) and the stress diffusivity  $\kappa$ , but does not depend on the spreading rate. The width scales as  $\sqrt{\kappa T}$ , so if the diffusivity is halved, it has a value of 90–100 km, and if the event frequency is doubled ( $T=50$  years), the effect on the width is the same.

Previously, we fitted the 1987–1990 displacements to those simulated assuming excitation by only the last episode (1975–1981). This is acceptable in the present case because most of the weight is laid on points relatively near the axis (within 50 km) and the contribution of the background velocity there is very small. Nevertheless, the background velocity may to some extent explain the discrepancy between the observed and simulated vectors in Figure 6 for the easternmost and westernmost points and points in the Askja region where past events are more recent, and therefore tectonic memory of them more significant.

## DISCUSSION

Plate motions are continuous in the plate interior. Near the boundary, however, there is a steady background movement which is, from time to time, overprinted by episodic movements, resulting in an averaged motion the same as in the plate interiors. The background movement is associated with deformation in the boundary zone as extensional stress is built up there. This stress is released in volcano-tectonic episodes that commence in a preexisting weak zone such as a fissure swarm in NE Iceland. The recurrence interval of episodes may be highly dependent on how weak the zone is, and therefore influenced by factors such as the presence of magma reservoirs in the fissure swarm.

Near the boundary (Figure 9a), the velocity alternates between accelerated periods (the stress relaxation stage) shortly after episodes and quiescent background movement periods (the stress buildup stage) between episodes. The latter periods are much longer than the former. Far from the

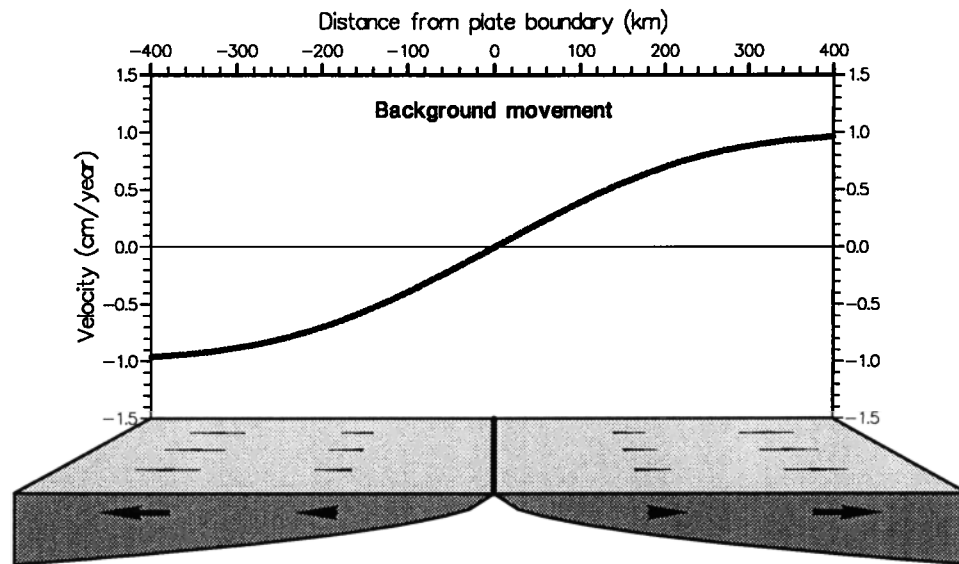


Fig. 10. Plate velocity as a function of distance from the divergent plate boundary resulting from past rifting episodes. Parameters are the same as used for Figure 9. Velocity is constant in the plate interior but is zero at the boundary where motion is purely episodic.

boundary, the plate velocity approaches the time-averaged velocity (Figure 9d). This means that if we measure movements in a plate boundary zone it is most likely that we will observe the stress buildup stage, that is, motion similar to the background movement. Figure 10 shows the velocity viewed from the plate boundary. If the same velocity field was viewed from the stable interior of one plate, the boundary zone of that plate would seem to move in the same direction as the other plate at smaller rates as though this zone was being “dragged away” by the other plate.

Movements along translational plate boundaries occur as strike-slip faulting. Those along convergent boundaries such as subduction zones occur as thrust faulting. These motions are also highly episodic in most cases and a similar stress diffusion mechanism must control the plate dynamics (although we do not yet have quantitative estimates of the stress diffusivities there). In all cases, a point near the plate boundary on one plate moves in the same direction as the other plate at a smaller rate. This rate is equal to the deficiency of the velocity there during the stress buildup stage.

Movements similar to those anticipated for the convergent boundary case have been reported by VLBI and satellite laser ranging (SLR). Kashima is a VLBI station on the Northeast Honshu Arc, Japan, whose movement has been monitored since 1984 [Heki *et al.*, 1987]. It is about 200 km from the Japan Trench, where the Pacific plate subducts beneath that arc. From the changing baseline length rates between Kashima and other VLBI stations, Heki *et al.* [1990] concluded that Kashima station, although located on the Eurasian plate, is moving with respect to its stable interior in the same direction as the subducting Pacific plate by about 2.6 cm/year. From 6 years of VLBI data in Alaska beginning in 1984, Ma *et al.* [1990] reported the northwestward movement of about 3.8 cm/year of Yakataga station, southeastern coastal Alaska, about 100 km from the trench (and smaller movements of a few other Alaskan stations) with respect to the Fairbanks station in the stable plate interior. By analyzing the baseline length change rates obtained by SLR, Harrison and Douglas [1990] estimated the

movement of Simosato station situated on the Southwest Honshu Arc, Japan (Eurasian plate) about 100 km from the Nankai Trough, where the Philippine Sea plate is subducting. This is about 3.8 cm/year with respect to the Eurasian plate and its direction is very similar to the Philippine Sea plate.

There are two possible interpretations for these observations: (1) permanent contraction of an island (continental) arc associated with active faulting and/or folding caused by compressional stress fields applied by a subducting oceanic plate [Heki *et al.*, 1990], and (2) elastic straining of the overriding plate due to a locked main thrust zone [Ma *et al.*, 1990]. In actual subduction zones, these two mechanisms are usually considered to occur with various relative contributions. This study provides support for the second mechanism and insight into its physical origin. In the plate interior, displacements caused by innumerable past large thrust earthquakes are diffused and stacked to produce movement at the time-averaged rate. Near the boundary, because the displacement caused by a single earthquake quickly diffuses away shortly after an earthquake, there is little movement measurable across the boundary, that is to say, the main thrust zone is locked. In all kinds of plate boundary where movement is episodic, during the stress buildup stage the strain is not completely taken up at a discrete boundary line, but some of it extends into the plates forming a plate boundary zone.

#### CONCLUDING REMARKS

In the aftermath of a major spreading episode on the plate boundary in NE Iceland, a major regional spatial strain-field was resolved. The GPS was used, and our observations would have been practically impossible using any other method. This work illustrates the power of the GPS to achieve new geophysical goals. A comparison of the results obtained using two different data processing packages and different analysts showed that in the case of good quality data the results were reassuringly similar. Interpretation of the results using a simple crustal model yielded a stress

diffusivity of about  $10 \text{ m}^2/\text{s}$ , and considerations of typical patterns of crustal structure throughout the world suggest that this value may be fairly uniform globally. The exceptionally low value we obtain for the Newtonian viscosity of the shallow layer of our model is qualitatively in keeping with what would be expected for a hotspot such as Iceland. Application of our results to study the predicted long-term crustal kinematics in the region around the plate boundary places constraints on the width of the boundary zone where plate movements are nonuniform. If global diffusivity is fairly uniform, then this width will depend mainly on the frequency of episodic movements. It will be interesting to extend this work to other types of plate boundaries.

#### APPENDIX

##### One-Dimensional Model

We assume a single thin elastic layer of thickness  $h$  overlying a viscous substrate of thickness  $b$  and viscosity  $\eta$ . We treat the source of the deformation as a single long vertical dike striking in the  $y$  direction, and let  $x$  be the horizontal distance from the dike and  $t$  be time. The problem is then one-dimensional with the only nonzero component of horizontal displacement,  $u(x, t)$ , lying in the  $x$  direction. The viscous traction at the base of the elastic layer is balanced by the elastic forces within it.

$$\frac{\eta}{b} \frac{\partial u}{\partial t} = h \frac{\partial \sigma_{xx}}{\partial x} \quad (\text{A1})$$

$\sigma_{xx}$  is the normal stress in the elastic layer in  $x$  direction (tension is positive). Because

$$\sigma_{xx} = M \frac{\partial u}{\partial x}$$

where  $M = 4\mu(\lambda + \mu)/(\lambda + 2\mu)$  is the elastic modulus relating horizontal stress and strain in the elastic layer for plane-stress conditions,  $u$  obeys the diffusion equation

$$\frac{\partial u}{\partial t} = \kappa \frac{\partial^2 u}{\partial x^2}, \quad (\text{A2})$$

where

$$\kappa = \frac{bhM}{\eta} \quad (\text{A3})$$

is the diffusivity.

Equation (A2) can be solved under various initial and boundary conditions by standard methods. Assume the elastic layer is initially at rest, and that at time  $t = 0$  a dike of width  $2U_0$  is intruded, so that parts of the elastic layer immediately adjacent to the line  $x = 0$  are suddenly displaced to the right or left by the amount  $U_0$ . Then the appropriate solution to the diffusion equation (A2) is

$$u(x, t) = U_0 \text{erfc} \frac{x}{2\sqrt{\kappa t}} \quad (\text{A4})$$

and the corresponding horizontal velocity is

$$\frac{\partial u}{\partial t} = \frac{U_0}{t\sqrt{\pi}} \frac{x}{2\sqrt{\kappa t}} e^{-x^2/4\kappa t}. \quad (\text{A5})$$

Figures A1 and A2 show  $u$  (displacement) and  $\partial u/\partial t$  (velocity) as functions of  $x$  (distance from the rift axis) at five different epochs (3, 6, 10, 20 and 50 years). A diffusivity

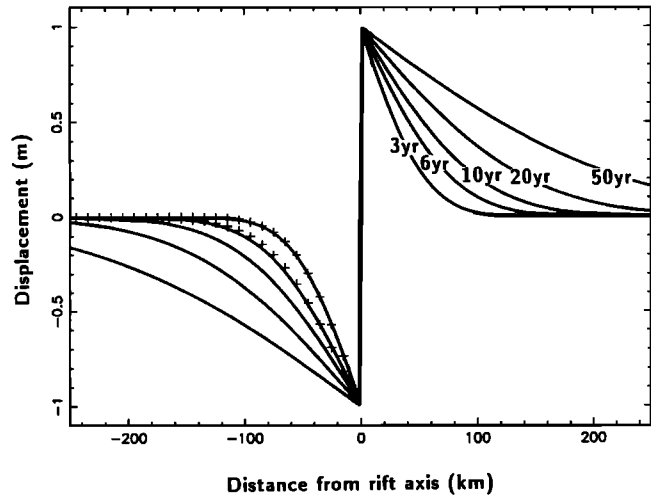


Fig. A1. Displacement of the eastern and western flanks of the plate boundary 3–50 years after the intrusion. Displacements are at first confined to the proximity of the boundary and then diffuse into the flanking plates. The curves are based on a one-dimensional model, a dike half width of 1 m and a stress diffusivity of  $10 \text{ m}^2/\text{s}$ . Displacements obtained by the two-dimensional finite difference simulation studies are indicated with pluses for comparison.

of  $10 \text{ m}^2/\text{s}$  and a  $U_0$  of 1 m are used. In early postrupture times, displacements are confined close to the rift axis (Figure A1) with a prominent velocity peak (Figure A2). The velocity peak migrates outward with time and decays in amplitude. At  $t = \infty$ , displacements are independent of distance from the dike ( $u = U_0$  for  $x > 0$ ,  $u = -U_0$  for  $x < 0$ ,  $\partial u/\partial t = 0$ ). Larger diffusivities ( $\kappa$ ) increase the migration rate of the peak.

This one-dimensional model is applicable only for a very long dike. To model the two-dimensional displacement field, we extend this theory to two dimensions.

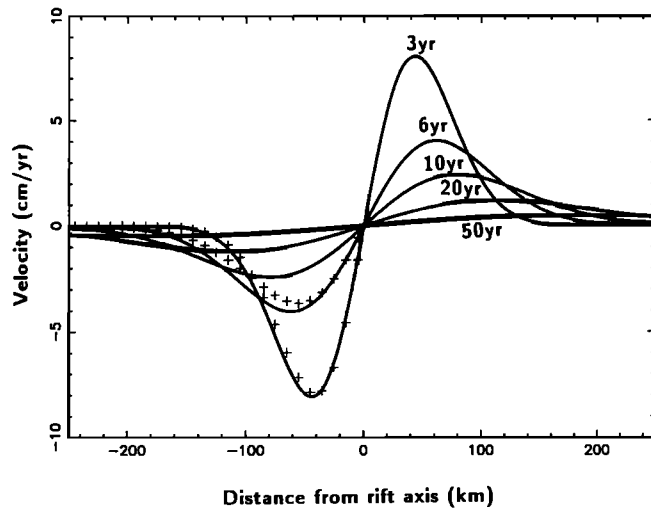


Fig. A2. Velocity in the eastern and western flanks of the plate boundary 3–50 years after the intrusion. Velocity peaks appear close to the boundary after the intrusion and propagate eastwards and westwards with diminishing amplitudes. The curves are based on a one-dimensional model, a dike half width of 1 m and a stress diffusivity of  $10 \text{ m}^2/\text{s}$ . Pluses are same as in Figure A1.



### Two-Dimensional Model

For a dike of finite length, the displacement vector has two horizontal components,  $u(x, y, t)$  in the  $x$  direction and  $v(x, y, t)$  in the  $y$  direction. The two-dimensional version of equation (A1) is

$$\frac{\eta}{b} \frac{\partial u}{\partial t} = h \left( \frac{\partial \sigma_{xx}}{\partial x} + \frac{\partial \sigma_{yx}}{\partial y} \right) \quad (\text{A6a})$$

$$\frac{\eta}{b} \frac{\partial v}{\partial t} = h \left( \frac{\partial \sigma_{yy}}{\partial y} + \frac{\partial \sigma_{xy}}{\partial x} \right) \quad (\text{A6b})$$

where  $\sigma_{xx}$  and  $\sigma_{yy}$  are the normal stresses in the  $x$  and  $y$  directions and  $\sigma_{xy}$  is the shear stress. We introduce a third axis  $z$  in the vertical direction and let  $w$  be the corresponding displacement component. The three-dimensional Hooke's law,

$$\sigma_{xx} = \lambda \Theta + 2\mu \frac{\partial u}{\partial x}$$

$$\sigma_{yy} = \lambda \Theta + 2\mu \frac{\partial v}{\partial y}$$

$$\sigma_{zz} = \lambda \Theta + 2\mu \frac{\partial w}{\partial z}$$

$$\sigma_{xy} = \mu \left( \frac{\partial u}{\partial y} + \frac{\partial v}{\partial x} \right)$$

$$\sigma_{yz} = \mu \left( \frac{\partial v}{\partial z} + \frac{\partial w}{\partial y} \right)$$

$$\sigma_{zx} = \mu \left( \frac{\partial w}{\partial x} + \frac{\partial u}{\partial z} \right)$$

where  $\Theta$  is the volume dilatation, and  $\lambda$  and  $\mu$  are the Lamé elastic moduli, is modified in the two-dimensional case by introducing plane-stress conditions ( $\sigma_{zz} = \sigma_{yz} = \sigma_{zx} = 0$ ).

$$\sigma_{xx} = \lambda' \left( \frac{\partial u}{\partial x} + \frac{\partial v}{\partial y} \right) + 2\mu \frac{\partial u}{\partial x} \quad (\text{A7a})$$

$$\sigma_{yy} = \lambda' \left( \frac{\partial u}{\partial x} + \frac{\partial v}{\partial y} \right) + 2\mu \frac{\partial v}{\partial y} \quad (\text{A7b})$$

$$\sigma_{xy} = \sigma_{yx} = \mu \left( \frac{\partial u}{\partial x} + \frac{\partial v}{\partial y} \right) \quad (\text{A7c})$$

$\lambda'$  and  $\Theta'$  are defined as

$$\lambda' \equiv \frac{2\lambda\mu}{\lambda + 2\mu} \quad (\text{A8})$$

$$\Theta' \equiv \frac{\partial u}{\partial x} + \frac{\partial v}{\partial y}. \quad (\text{A9})$$

Then the equation (A6) becomes

$$\frac{\partial u}{\partial t} = \kappa_1 \frac{\partial^2 u}{\partial x^2} + \kappa_2 \frac{\partial^2 v}{\partial x \partial y} + \kappa_3 \frac{\partial^2 u}{\partial y^2} \quad (\text{A10a})$$

$$\frac{\partial v}{\partial t} = \kappa_1 \frac{\partial^2 v}{\partial y^2} + \kappa_2 \frac{\partial^2 u}{\partial y \partial x} + \kappa_3 \frac{\partial^2 v}{\partial x^2} \quad (\text{A10b})$$

with

$$\kappa_1 \equiv (\lambda' + 2\mu)bh/\eta \quad \kappa_2 \equiv (\lambda' + \mu)bh/\eta \quad \kappa_3 \equiv \mu bh/\eta$$

where  $\kappa_1$  has the same value as  $\kappa$  in the one-dimensional case (equation (A3)). If  $\lambda = \mu$  (Poisson's ratio = 0.25) then the ratio  $\kappa_1:\kappa_2:\kappa_3$  is 8:5:3. This changes slightly if  $\lambda$  and  $\mu$  are not equal, and becomes 12:7:5 when  $\lambda$  is half of  $\mu$  (Poisson's ratio = 0.33). The vertical strain is

$$e_{zz} = -\frac{\lambda}{\lambda + 2\mu} \Theta'. \quad (\text{A11})$$

Instantaneous uplift or subsidence (i.e., no isostatic rebound) is obtained by multiplying  $e_{zz}$  by the elastic layer thickness  $h$ .

### Integration of the Partial Differential Equations

Equations (A10) can be integrated using the finite difference method. Consider a rectangular area and introduce discretized values  $u_{i,j}^{(k)}$  and  $v_{i,j}^{(k)}$  of the continuous functions  $u(x, y, t)$  and  $v(x, y, t)$ . Variables  $i, j$  and  $k$  represent the  $x$  and  $y$  coordinates and time  $t$ , respectively. Then equations (A10a) and (A10b) are approximated by

$$\begin{aligned} \frac{u_{i,j}^{(k+1)} - u_{i,j}^{(k)}}{\Delta t} &= \kappa_1 \frac{u_{i+1,j}^{(k)} - 2u_{i,j}^{(k)} + u_{i-1,j}^{(k)}}{\Delta x^2} \\ &+ \kappa_2 \frac{v_{i+1,j+1}^{(k)} - v_{i+1,j-1}^{(k)} - v_{i-1,j+1}^{(k)} + v_{i-1,j-1}^{(k)}}{2\Delta x \cdot 2\Delta y} \\ &+ \kappa_3 \frac{u_{i,j+1}^{(k)} - 2u_{i,j}^{(k)} + u_{i,j-1}^{(k)}}{\Delta y^2} \end{aligned} \quad (\text{A12a})$$

$$\begin{aligned} \frac{v_{i,j}^{(k+1)} - v_{i,j}^{(k)}}{\Delta t} &= \kappa_1 \frac{v_{i,j+1}^{(k)} - 2v_{i,j}^{(k)} + v_{i,j-1}^{(k)}}{\Delta y^2} \\ &+ \kappa_2 \frac{u_{i+1,j+1}^{(k)} - u_{i+1,j-1}^{(k)} - u_{i-1,j+1}^{(k)} + u_{i-1,j-1}^{(k)}}{2\Delta x \cdot 2\Delta y} \\ &+ \kappa_3 \frac{v_{i+1,j}^{(k)} - 2v_{i,j}^{(k)} + v_{i-1,j}^{(k)}}{\Delta x^2} \end{aligned} \quad (\text{A12b})$$

where  $\Delta t$  is the time step and  $\Delta x$  and  $\Delta y$  are the point separations in the  $x$  and  $y$  directions. Using this approximation, the values of  $u$  and  $v$  at the  $(k+1)$ th epoch may be calculated explicitly from the values at the  $k$ th epoch. The values at any epoch are obtained by repeating this step from appropriate initial conditions.

The finite difference scheme was tested for two extreme cases, that is,  $t = \infty$  and  $t \ll \infty$  assuming a rectangular dike, 1 m thick and 100 km long. The two-dimensional analytic solution for the displacement field caused by a displacement discontinuity [e.g., *Crouch and Starfield, 1983*] represents the situation at  $t = \infty$ . If we adopt the same boundary conditions, equation (A12) should give a similar displacement field after sufficient calculation steps. This was the case to the millimeter level. For the case  $t \ll \infty$ , the displacement field close to the dike center should coincide with that calculated using the analytic solution (equation (A4)) for the one-dimensional case. We confirmed the coincidences for two epochs, 3 and 6 years after the intrusion (Figures A1 and A2).

The computation grid (Figure 2) was made large enough to justify using zero displacement as the remote boundary condition. Along the dike axis ( $x = 0$ ), the following boundary condition was imposed.

$$\sigma_{xy} = \frac{1}{2} \left( \frac{\partial u}{\partial y} + \frac{\partial v}{\partial x} \right) = 0$$

$\Delta x$  and  $\Delta y$  were made small enough (6 km) to get reasonable resolution.  $\Delta t$  was made small enough (typically a few days) to ensure numerical calculation stability.

Dikes were assumed to have been intruded as six discrete units whose shapes are illustrated in Figure A3 (the "low estimate" of Tryggvason [1984]). This model is based on ground surveying using geodimeters [Tryggvason, 1984]. Several minor events were merged into single events (e.g., "1976 Oct" represents two events that occurred in October 1976 and January 1977). Errors introduced by these approximations will be relatively minor because we are interested in the deformation field about 10 years after these events. We ignored volcanic activity after 1981 because no appreciable crustal widening occurred. No initial movements were assumed parallel to the dikes; the dike-parallel motion is one of the products of the stress diffusion computation.

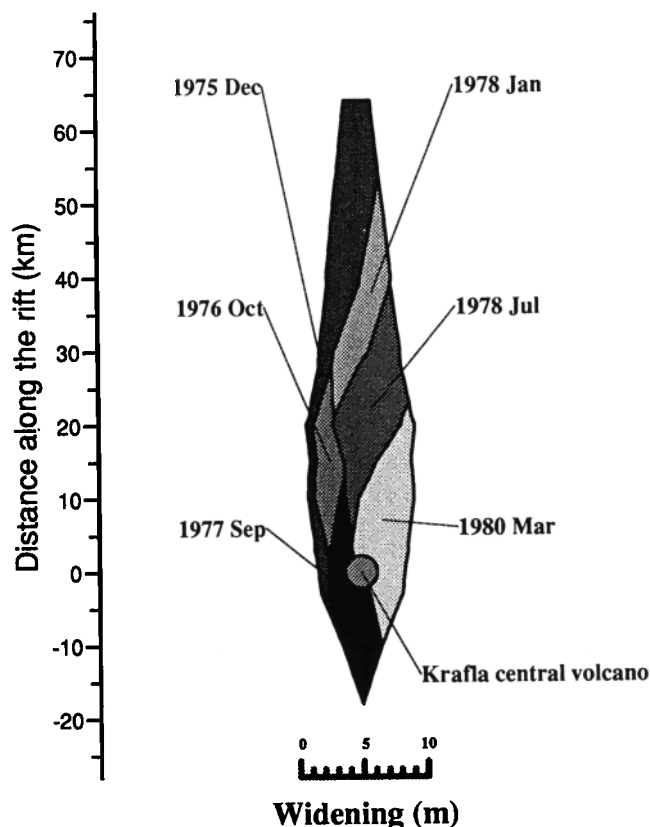


Fig. A3. Shapes of the dikes used in the finite difference calculation. Dike widths are based on ground geodetic surveys, but the part north of the Krafla center could be wider by a few meters because no measurements were made prior to the first event [Tryggvason, 1984]. Intrusion actually occurred as more than 10 pulses, but some of the minor events are bundled together giving six major events between December 1975 and March 1980. The abrupt termination of the dike at the northern end coincides with the junction with the Grímsey fault within the Tjörnes Fracture Zone.

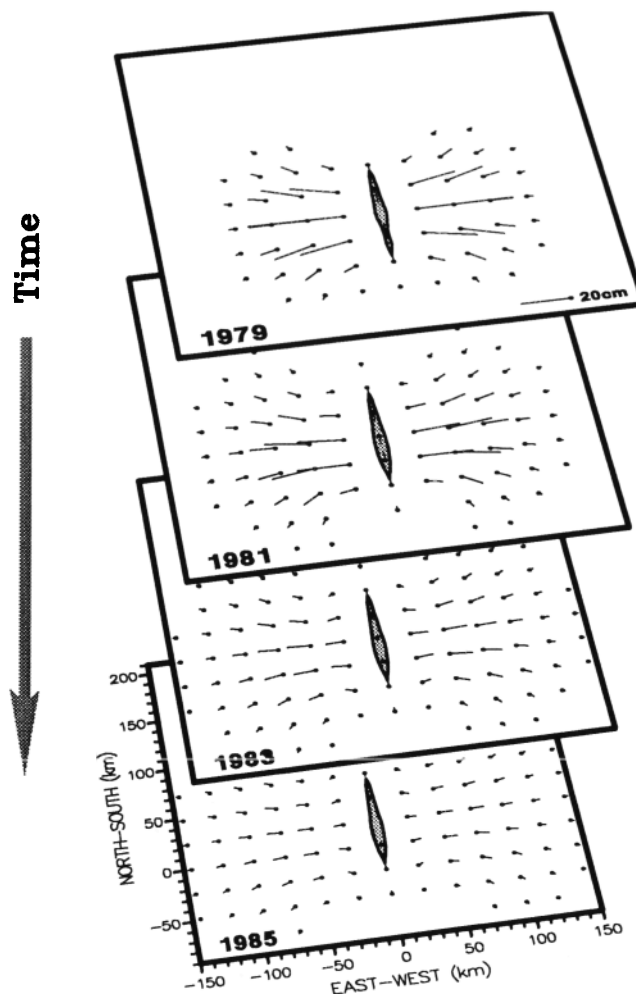


Fig. A4. Evolution of the displacement field after the Krafla rifting episode, simulated using the finite difference method. Lines indicate cumulative movements in 1 year (e.g., from January 1, 1981, to December 31, 1981, for "1981"). Only displacements larger than 1 cm are displayed. Four different epochs from 1979 to 1985 are shown. Diffusivity,  $\kappa_1$ , is assumed to be  $10 \text{ m}^2/\text{s}$ .

Variables  $u_{i,j}^{(k)}$  and  $v_{i,j}^{(k)}$  are set to zero for all  $i$  and  $j$  at the start ( $k = 0$ ). When the time  $k$  reaches one of the dike opening events, the corresponding displacements (Figure A3) were added to  $u_{i,j}^{(k)}$  on the rift axis ( $i = 0$ ) at appropriate  $j$ . The displacements during a specific interval are obtained as differences of the values at the beginning and the end of the period. Figure A4 shows the displacements for 1-year intervals at four different epochs. Variable  $u$  (the rift-normal displacement) has a general trend similar to the one-dimensional model. In addition, however, rift-parallel movements occur, introducing an along-dike contraction near the axis and a radial pattern of displacement far from the dike axis. Figure A4 uses values of  $\kappa_1 = 10.0 \text{ m}^2/\text{s}$  and  $\lambda = \mu$ , so the other two diffusivities are  $\kappa_2 \approx 6.2 \text{ m}^2/\text{s}$ ,  $\kappa_3 \approx 3.8 \text{ m}^2/\text{s}$ .

**Acknowledgments.** The authors wish to thank the crews of the GPS surveys in 1987 and 1990. These surveys were conducted by collaboration of University of Durham (England), Universität Hannover (Germany) and Icelandic GPS Coordinating Committee. The contribution of the University of Durham was financed by NERC grants GR3/6676 and GR9/161 and a grant from the Wolfson Foundation. The contribution of the Universität Han-

nover was financed by DFG grants Se 313/8-1, Se 313/8-2 and Se 313/8-3. Wojciech J. Zakrzewski and Jim Dieterich kindly contributed to discussions about the boundary conditions. Reviews by Páll Einarsson and one anonymous referee considerably improved the paper.

## REFERENCES

- Beblo, M., A. Björnsson, K. Arnason, B. Stein, and P. Wolfgram, Electrical conductivity beneath Iceland—Constraints imposed by magnetotelluric results on temperature, partial melt, crust and mantle structure, *J. Geophys.*, *53*, 16–23, 1983.
- Björnsson, A., Dynamics of crustal rifting in NE Iceland, *J. Geophys. Res.*, *90*, 10,151–10,162, 1985.
- Björnsson, A., K. Saemundsson, P. Einarsson, E. Tryggvason, and K. Gronvold, Current rifting episode in North Iceland, *Nature*, *266*, 318–323, 1977.
- Björnsson, A., G. Johnsen, S. Sigurdsson, G. Thorbergsson, and E. Tryggvason, Rifting of the plate boundary in North Iceland 1975–1978, *J. Geophys. Res.*, *84*, 3029–3038, 1979.
- Blewitt, G., An automatic editing algorithm for GPS data, *Geophys. Res. Lett.*, *17*, 199–202, 1990.
- Bott, M.H.P., and D.S. Dean, Stress diffusion from plate boundaries, *Nature*, *243*, 339–341, 1973.
- Carter, W. E., and D. S. Robertson, Definition of a terrestrial reference frame using IRIS VLBI observations: Approaching millimeter accuracy, paper presented at Symposium 105, IAG General Meeting, Int. Assoc. Geod., Edinburgh, Scotland, 1989.
- Crouch, S.L., and A.M. Starfield, *Boundary Element Methods in Solid Mechanics*, Allen and Unwin, Winchester, Mass., 1983.
- DeMets, C., R. G. Gordon, D. F. Argus, and S. Stein, Current plate motions, *Geophys. J. Int.*, *101*, 425–478, 1990.
- Einarsson, P., Earthquakes and present-day tectonism in Iceland, *Tectonophysics*, *189*, 261–279, 1991.
- Elsasser, W.M., Convection and stress propagation in the upper mantle, in *The Application of Modern Physics to the Earth and Planetary Interiors*, edited by S.K. Runcorn, pp. 223–246, Wiley-Interscience, New York, 1969.
- Foulger, G.R., C.-H. Jahn, G. Seeber, P. Einarsson, B.R. Julian, and K. Heki, Post rifting stress relaxation at the accretionary plate boundary in Iceland, measured using the Global Positioning System, *Nature*, *358*, 488–490, 1992.
- Harrison, C.G.A., and N.B. Douglas, Satellite laser ranging and geological constraints on plate motion, *Tectonics*, *9*, 935–952, 1990.
- Heki, K., Three approaches to improve the estimation accuracies of the vertical VLBI station positions, *J. Geod. Soc. Jpn.*, *36*, 143–154, 1990.
- Heki, K., A network adjustment program for the Bernese Global Positioning System data analysis software, *J. Geod. Soc. Jpn.*, *38*, 309–312, 1992.
- Heki, K., Y. Takahashi, T. Kondo, N. Kawaguchi, F. Takahashi, and N. Kawano, The relative movement of the North American and Pacific plates in 1984–1985, detected by the Pacific VLBI network, *Tectonophysics*, *144*, 151–158, 1987.
- Heki, K., Y. Takahashi, and T. Kondo, Contraction of north-eastern Japan: Evidence from horizontal displacement of a Japanese station in global very long baseline interferometry networks, *Tectonophysics*, *181*, 113–122, 1990.
- Heki, K., G. R. Foulger, O. Alp, and M. Ergün, 1989 GPS campaign in Southwest Turkey - Data analysis, paper presented at International Association of Geodesy Symposium G-2, IUGG XX General Assembly, Int. Union of Geod. and Geophys., Vienna, 1991.
- Jahn, C.-H., G. Seeber, G.R. Foulger, and A. Björnsson, A GPS survey in the north-east volcanic zone, Iceland 1987 - First results, in *Proceedings of the General Meeting of International Association of Geodesy Edinburgh, Global and Regional Geodynamics*, pp. 173–181, Springer Verlag, New York, 1990.
- Jahn, C.-H., G. Seeber, G.R. Foulger, and P. Einarsson, GPS epoch measurements across the mid-Atlantic plate boundary in northern Iceland 1987–1990, paper presented at Union Symposium U-5, IUGG XX General Assembly, Int. Union of Geod. and Geophys., Vienna, 1991.
- Johnson, G.L., and S.P. Jakobsson, Structure and petrology of the Reykjanes Ridge between 62° 55'N and 63° 48'N, *J. Geophys. Res.*, *90*, 10,073–10,083, 1985.
- Ma, C., J.M. Sauber, L.J. Bell, T.A. Clark, D. Gordon, W.E. Himwich, and J.W. Ryan, Measurement of horizontal motions in Alaska using very long baseline interferometry, *J. Geophys. Res.*, *95*, 21,991–22,011, 1990.
- Minster, J. B., and T. H. Jordan, Present-day plate motions, *J. Geophys. Res.*, *83*, 5331–5354, 1978.
- Möller, D., and B. Ritter, Geodetic measurements and horizontal crustal movements in the rift zone of NE Iceland, *J. Geophys.*, *47*, 110–119, 1980.
- Ranalli, G., Viscosity of the asthenosphere, *Nature*, *361*, 211, 1993.
- Rothacher, M., G. Beutler, W. Gurtner, T. Schildknecht and U. Wild, *Documentation for Bernese GPS Software Version 3.2*, University of Bern, Bern, 1990.
- Ruegg, J.C., and M. Kasser, Deformation across the Asal-Ghoubbet rift, Djibouti, uplift and crustal extension 1979–1986, *Geophys. Res. Lett.*, *14*, 745–748, 1987.
- Saemundsson, K., Evolution of the axial rifting zone in northern Iceland and the Tjörnes Fracture Zone, *Geol. Soc. Am. Bull.*, *85*, 495–504, 1974.
- Savage, J.C., and W.H. Prescott, Comment on “Nonlinear stress propagation in the Earth's upper mantle” by H.J. Melosh, *J. Geophys. Res.*, *83*, 5005–5007, 1978.
- Sigmundsson, F., Post-glacial rebound and asthenospheric viscosity in Iceland, *Geophys. Res. Lett.*, *18*, 1131–1134, 1991.
- Sigurdsson, H., and R. S. J. Sparks, Rifting episode in north Iceland in 1874–1875 and the eruption of Askja and Sveinagjá, *Bull. Volcanol.*, *41*, 149–167, 1978.
- Tryggvason, E., Widening of the Krafla fissure swarm during the 1975–1981 volcano-tectonic episode, *Bull. Volcanol.*, *47*, 47–69, 1984.
- Wendt, K., D. Möller, and B. Ritter, Geodetic measurements of surface deformations during the present rifting episode in NE Iceland, *J. Geophys. Res.*, *90*, 10,163–10,172, 1985.
- Wübbena, G., The GPS adjustment software package - GEONAP - Concepts and models, paper presented at the Fifth International Geodetic Symposium on Satellite Positioning, Defense Mapping Agency and National Geodetic Survey, Las Cruces, N. M., 1989.

G.R. Foulger and B.R. Julian, U. S. Geological Survey, 345 Middlefield Rd., MS977, Menlo Park, CA 94025.

K. Heki, Kashima Space Research Center, Communications Research Laboratory, 893-1 Hirai, Kashima, Ibaraki 314, Japan.

C.-H. Jahn, Institut für Erdmessung, Universität Hannover, D-3000 Hannover 1, Nienburger Str. 5, Germany.

(Received July 13, 1992;  
revised February 25, 1993;  
accepted March 23, 1993.)